Leckie, R.M., Sigurdsson, H., Acton, G.D., and Draper, G. (Eds.), 2000
Proceedings of the Ocean Drilling Program, Scientific Results, Vol. 165

9. PALEOLATITUDE OF THE CARIBBEAN PLATE SINCE THE LATE CRETACEOUS[1]

Gary D. Acton,[2] Bruno Galbrun,[3] and John W. King[4]

ABSTRACT

We used paleomagnetic results from Sites 998, 999, 1000, and 1001 to estimate the paleolatitude of the Caribbean region over the past 80 m.y. The data include remanence measurements of split-core sections (typically 1.5 m long) and discrete samples (6–12 cm^3 in volume) from volcanic and sedimentary rocks. From these, we computed 15 new paleolatitude estimates for Sites 999 and 1001 on the Caribbean plate and three new paleolatitude estimates for Site 998 on the Cayman Rise, currently on the southern North American plate. One estimate from Site 1001 is based on 230 measurements made along split-core sections of basalt after demagnetization of 20–25 mT. The other 17 estimates are based on principal component analysis of demagnetization data from 438 discrete paleomagnetic samples from sedimentary units. Where necessary, the 18 new paleolatitude estimates are corrected for a polarity ambiguity bias that occurs when averaging paleomagnetic data from drill cores that have shallow inclinations and are not azimuthally oriented. We also investigated the contribution of additional biases that may arise from a compaction-related inclination error, which could affect the sedimentary units, though not the basalt units. Several lines of evidence, including the lack of a correlation between porosity (or water content) and inclination, indicate that the inclination error is small, if present at all.

The results from Sites 999 and 1001 indicate that the Caribbean plate was 5°–15° south of its current position at ~80 Ma, possibly placing it directly over the equator in the Late Cretaceous. Although the data do not preclude changes in the rate of northward motion over the past 80 m.y., they are consistent with a constant northward progression at a rate of 18 km/m.y. Given the uncertainties in the data, rates of northward motion could be as low as 8 km/m.y. or as high as 22 km/m.y. These results are compatible with several existing models for the evolution of the Caribbean plate, including those that have the Caribbean plate originating in the Pacific Ocean west of subduction zones active in the Central American region during the Cretaceous, and those that have the Caribbean plate originating within the Central American region, though more than 1000 km west of its current position relative to North and South America.

INTRODUCTION

The Caribbean plate currently lies between the North and South American plates at a latitude between 10°N and 18°N (Fig. 1). From a plate tectonic perspective, it is extremely unlikely that the small Caribbean plate has maintained this position over time, particularly since all the larger bounding plates have been in motion.

Recent plate motions, estimated from earthquake slip vectors and seafloor spreading rates, give a broad range of directions and motions for the Caribbean plate. For instance, at a point (18°N, 278°E) near the Cayman Rise, the NUVEL-1A global plate motion model predicts that the Caribbean plate is moving N77°E at a rate of 11 mm/yr relative to North America (DeMets et al., 1994). In contrast, estimates that use data directly from Caribbean plate boundaries indicate that the relative motion is more easterly (N80°E) and two to three times faster (20–37 mm/yr) (e.g., Sykes et al., 1982; Deng and Sykes, 1995). To ascertain the absolute motion of the Caribbean plate, these relative motions can be combined with the motion of North America relative to the hot spots. In the hot-spot reference frame, the North American plate is moving N250°E at a rate of 31 km/m.y. (Gripp and Gordon, 1990). Within the uncertainties of the relative and absolute motion estimates, the Caribbean plate could be moving either east-northeast at rates of up to ~10 km/m.y. or west-southwest at rates of up to 20 km/m.y. over the past few million years.

Global Positioning System (GPS) measurements spanning the past 12 yr have begun to give more precise relative and absolute motion estimates, though these too have interpretational flexibility because the Caribbean GPS sites are limited to islands that in some cases are likely part of a plate boundary zone rather than the Caribbean plate. From the Euler vector given by Dixon et al. (1998), which is at 18.6°N, 107.2°E with a rotation rate of 0.36°/m.y., the Caribbean plate is moving N76°E at 24 mm/yr relative to North America. When placed in the International Terrestrial Reference Frame (ITRF-94; Boucher et al., 1996), the four GPS sites—Capotillo, Hispaniola; Cabo Frances Viejo, Hispaniola; Cabo Rojo, Hispaniola; and Isabela, Puerto Rico—considered to be on the northern Caribbean plate—move on average N47°E at a rate of 8 mm/yr (computed from table 5 of Dixon et al., 1998). The ITRF was designed to agree on average with the absolute plate motions of Argus and Gordon (1991), which assume no net rotation of the lithosphere. Assuming no true polar wander, this estimate would suggest that the Caribbean plate is currently moving northward at 5.4 mm/yr.

The position and motion of the Caribbean plate prior to recent times is even more poorly constrained because the plate boundary zones are complex and mainly destructive (strike-slip boundaries with components of extension and compression and subduction zones) and hot-spot tracks are absent. Paleomagnetic data are also very sparse from within the Caribbean plate (e.g., Kent and Spariosu, 1982; Gose, 1985; MacDonald, 1990), so much so that no Caribbean apparent polar wander path can be constructed and only crude estimates of the paleolatitude of the plate can be made. Many more data come from the margins of the plate (e.g., Gose, 1983, 1985; Beck, 1988; MacDonald, 1990; Frisch et al., 1992; Burmester et al., 1996), but these are from crustal blocks that show a variety of vertical axis rotations and latitudinal translations. Extracting an apparent polar wander path from these crustal blocks would, therefore, be nearly impossible because each crustal block likely has a unique history of moving relative to and docking with the Caribbean plate.

[1]Leckie, R.M., Sigurdsson, H., Acton, G.D., and Draper, G. (Eds.), 2000. *Proc. ODP, Sci. Results,* 165: College Station, TX (Ocean Drilling Program).
[2]Ocean Drilling Program, Texas A&M University, 1000 Discovery Drive, College Station, TX 77845-9547, U.S.A. acton@odpemail.tamu.edu
[3]Laboratoire de Stratigraphie - UA CNRS 1315, Universite Pierre et Marie Curie, 4 Place Jussieu, Paris, Cedex, 75252, France.
[4]Graduate School of Oceanography, University of Rhode Island, Narragansett Bay Campus, Narragansett, RI 02882-1197, U.S.A.

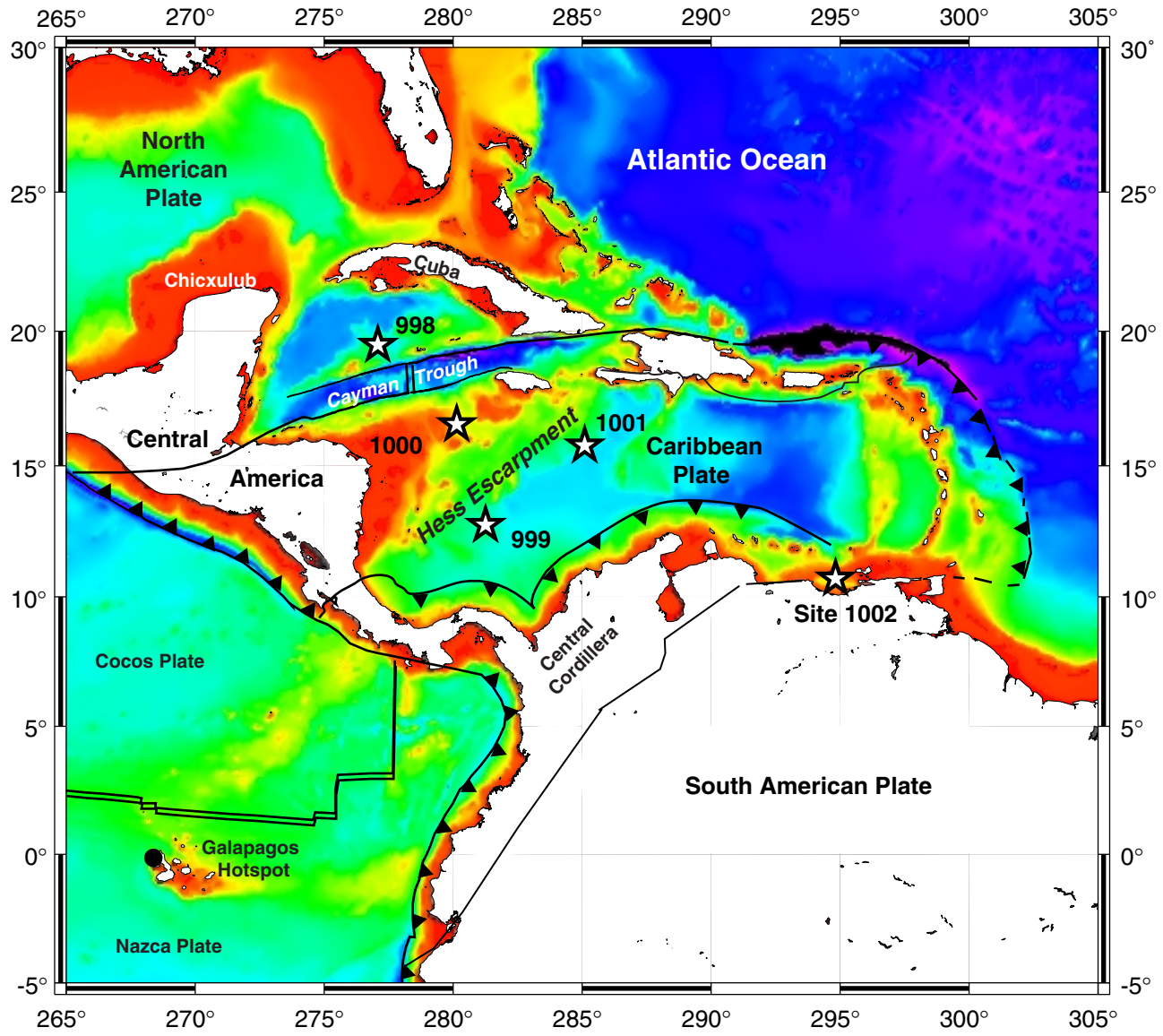

Figure 1. Location of Leg 165 drill sites (stars) and plate boundaries for the Caribbean plate (black lines: spreading centers are shown with two parallel lines, subduction zones with triangles attached, and strike-slip or uncertain boundaries as single lines). The plate boundaries are similar to those shown in Draper et al. (1994) and Meschede and Frisch (1998). The actual plate boundaries in several areas are more diffuse and complex than those shown. The solid dot gives the approximate location of the Galapagos hot spot.

Data are very sparse, however, from directly on the Caribbean plate. In the compilation of Caribbean paleomagnetic data by MacDonald (1990), the sum of all Caribbean basin data of pre-Miocene age came from just 34 specimens from five Deep Sea Drilling Project (DSDP) sites analyzed by Lowrie and Opdyke (1973). These Late Cretaceous specimens indicated a paleolatitude 5°–10° less than that of the present latitude of the DSDP sites, but were too few to establish a convincing paleolatitude estimate. Similarly, a paleomagnetic pole computed from the magnetic anomaly over a presumably Late Cretaceous-age seamount near DSDP Site 145 indicates a near equatorial position for the Caribbean plate (Raff, 1973). Likewise, paleomagnetic inclinations from Late Cretaceous- to Eocene-age rock units in Central America that are now part of the Caribbean plate indicate near-equatorial paleolatitudes (Gose, 1983; Frisch et al., 1992).

Taken together, the recent plate motion estimates and the sparse paleomagnetic data suggest a more southerly position for the Caribbean plate since the Late Cretaceous. The latitude and the rate of northward motion over the interval from Late Cretaceous until recent times are, however, largely unconstrained.

Here we present results from paleomagnetic measurements from Leg 165 cores, including three sites (Sites 999, 1000, and 1001) from the Caribbean plate and one (Site 998) from the Cayman Rise, just to the north of the Caribbean plate. The new data expand the number of paleomagnetic results from pre-Miocene rocks from the Caribbean basin by more than an order of magnitude and constrain the paleolatitude of the Caribbean plate over the past 80 m.y. These constraints are then compared against tectonic models for the evolution of the Caribbean plate.

GEOLOGIC SETTING, LITHOLOGIES, AND AGES

We have focused our study on the four sites (Sites 998–1001) cored during Leg 165 where sedimentary sections older than Pleis-

tocene age were penetrated. At Site 1001, we also cored through 37 m of Upper Cretaceous basaltic basement. An extensive description of the coring results, including lithologic descriptions, core photos, and preliminary biostratigraphic and paleontological analyses are presented within the Ocean Drilling Program (ODP) *Initial Reports* Volume 165 (Sigurdsson, Leckie, Acton, et al., 1997). Core photos and detailed core descriptions presented at the end of that volume can be used to determine the position and lithology of our samples, which follow the standard ODP sample naming convention. Below we present a brief summary of some of the relevant aspects of the sections sampled in this study, including their geologic setting, lithologies, ages, and sedimentation rates.

Site 998 (19.49°N, 277.06°E) is located on the Cayman Rise, north of the Cayman Ridge and Cayman Trough (Fig. 1). It thus lies on the southern portion of the North American plate rather than on the Caribbean plate. A sedimentary section spanning the lower Eocene (~52 Ma) to the present was recovered from coring in two holes, the deepest of which penetrated 904.8 meters below seafloor (mbsf). This section consists mainly of carbonates with varying amounts of clay and ash. Discrete clay-rich layers and ash layers are present throughout. The upper 160 m of the section is composed mainly of oozes (nannofossil and foraminiferal) and clayey nannofossil mixed sediments. Below 160 mbsf, the dominant lithologies are nannofossil chalks that grade into limestone with clay at ~700 mbsf. Sedimentation rates vary between 8 and 30 m/m.y., averaging ~17 m/m.y. (1.7 cm/k.y.) over the 52 m.y. interval.

Site 999 (12.74°N, 281.26°E) is located in the Colombian Basin, southeast of the Hess Escarpment. A sedimentary section spanning the upper Maastrichtian (~66 Ma) to the present was recovered from coring in two holes, the deepest of which penetrated 1066.4 mbsf. The upper 347 m of the section consists mainly of clay-rich carbonates classified as nannofossil and foraminiferal clayey mixed sediments. From 347 to 566 mbsf, clayey chalk with foraminifers and nannofossils is the main lithology. Below this the dominant lithology is clayey limestone except for an interval of clayey calcareous mixed sedimentary rock from 887 to 1033 mbsf. Discrete ash layers are found throughout the section. Sedimentation rates vary between 6 and 32 m/m.y., averaging ~16 m/m.y. (1.6 cm/k.y.) over the 66 m.y. interval.

Site 1000 (16.55°N, 280.13°E) is located on the northern Nicaraguan Rise, ~265 km southwest of Jamaica. A sedimentary section spanning the lower Miocene (~19 Ma) to the present was recovered from coring in two holes, the deepest of which penetrated 696 mbsf. The entire section is carbonate rich with the upper 307 m being dominantly nannofossil and micritic oozes, the interval from 370 to 513 mbsf is dominantly micritic nannofossil chalk, and the lower interval is dominantly limestone. Discrete ash layers are present throughout the section. Sedimentation rates vary between 27 and 47 m/m.y., averaging ~37 m/m.y. (3.7 cm/k.y.) over the 19-m.y. interval.

Site 1001 (15.76°N, 285.09°E) is located on the Hess Escarpment, on part of the lower Nicaraguan Rise. Basaltic basement (~81 Ma) and a sedimentary section spanning the Campanian to the present was recovered from coring in two holes, the deepest of which penetrated 522.8 mbsf. The upper 165.7 m, which is dominantly clayey nannofossil ooze, clayey nannofossil mixed sediment, and nannofossil ooze, extends down to the middle Miocene. The middle Miocene nannofossil ooze is separated from the underlying early Eocene–Campanian-age section by 28 cm of Eocene chalk and two unconformities with a total duration of 38 m.y. From 166 to 352 mbsf, the early Eocene–late Paleocene-age section is composed of chalk and mixed sedimentary rock with clay. A 10- to 20-cm-thick K/T boundary interval was recovered from both Holes 1001A and 1001B at 352–353 mbsf. The Upper Cretaceous sediments down to 473 mbsf are limestones and claystones. From 473 to 485 mbsf, in the interval just above igneous basement, there is a significant reduction in carbonate and an increase in volcaniclastic material, including ash layers and several thick ash turbidites. The very base of this interval contains subangular fragments of basaltic lapilli and hyaloclastite breccia. As at the other sites, discrete ash layers are present throughout the sedimentary section. Sedimentation rates vary between ~4 and 30 m/m.y., averaging ~12 m/m.y. (1.2 cm/k.y.) in the Neogene, 14 m/m.y. (1.4 cm/k.y.) in the Paleogene, and 11 m/m.y. (1.1 cm/k.y.) in the Cretaceous.

At Site 1001, we also cored through igneous basement from ~485 mbsf to the bottom of both holes. In Hole 1001A we penetrated 37 m into basement and recovered 20 m of igneous rock (54% recovery), whereas we penetrated only ~3 m into basement with 2.1 m of recovery in Hole 1001B. The basement is probably wholly extrusive in origin and the dominant lithologies are vesicular and massive basalts.

During Leg 165, the basement in Hole 1001B was subdivided into 12 formations, which were thought to be representative of individual lava flows or groups of similar flows and associated hyaloclastite breccias (Sigurdsson, Leckie, Acton, et al., 1997). The formation divisions where based mainly on chilled margins in the form of glassy rinds or on the presence of hyaloclastite breccias or carbonate deposits between formations. The formations were further subdivided into 52 units at coring gaps where changes in texture or composition occurred, some of which were quite subtle (pp. 325–329 and 739–763 in Sigurdsson, Leckie, Acton, et al., 1997). Separating the recovered basalts into independent flows is subjective. We consider several of the units from within a formation as individual lava flows and note that additional subdivision may be necessary between cores, where coring gaps are typically the largest.

Because of the importance of subdividing the extrusive rocks into individual flows that might have sampled the geomagnetic field independently, we present our own "flow unit" picks (Table 1). The flow-unit boundaries, as described in Table 1, are typically at chilled margins, though some of the chilled margins could be the margins of basalt pillows that belong to a single thicker basalt flow. Each of our 27 flow units potentially could represent flows that were extruded far enough apart in time that they could possibly provide independent samples of the geomagnetic field. More likely multiple flow units have been extruded within a short time interval relative to geomagnetic secular variation (SV), which indeed proved to be the case as discussed below. Relative to the subdivision derived during Leg 165 (Sigurdsson, Leckie, Acton, et al., 1997), we have more flow units than formations because we have intentionally subdivided any potentially independent flow from its juxtaposing flows when there was any indication of independence (chilled margins, change of texture across core boundaries, or change in inclination across a coring gap). We also have fewer flow units than the unit subdivision of Sigurdsson, Leckie, Acton, et al. (1997) because their units include breccia intervals and hyaloclastite intervals that were not sampled for paleomagnetic purposes.

Ages

We present our paleomagnetic results first as a function of depth, and then convert these to ages using calcareous nannofossil and foraminiferal datums. We use the datums given in Sigurdsson, Leckie, Acton, et al. (1997) except where they have been superseded by publications within this volume. In particular, the Neogene calcareous nannofossil ages for Sites 998, 999, and 1000 come from Kameo and Bralower (Chap. 1, this volume), and the Neogene planktonic foraminifer ages at Site 999 come from Chaisson and D'Hondt (Chap. 2, this volume).

^{40}Ar–^{39}Ar dates of three basalt samples from Hole 1001A give an age of 81 ± 1 Ma for the basement (Sinton et al., Chap.15, this volume). This age is in good agreement with the 76–80 Ma age obtained from nannofossil and foraminiferal datums from the overlying sediments (Sigurdsson, Leckie, Acton, et al., 1997).

PALEOMAGNETIC DATA AND ANALYSIS

A variety of rock types, sample sizes, magnetometers, and demagnetization techniques were used in this study. Each data type has strengths and weaknesses, which when recognized can be used to obtain accurate paleomagnetic estimates within the uncertainty bounds. In this section, we outline the laboratory methods used to obtain the raw paleomagnetic observations and the analysis methods used for estimating paleolatitudes.

We also provide a complete archive of the data in the tables included on the CD-ROM (see back pocket, this volume). The data include shipboard split-core data that are available through ODP, but were not archived in the Leg 165 *Initial Reports* volume, as well as data collected since Leg 165. Table 2 lists the contents of the tables on the CD-ROM (Tables 3–18).

Long-Core Results from Shipboard Measurements

The laboratory methods and results of shipboard paleomagnetic measurements are described in detail in Sigurdsson, Leckie, Acton, et al. (1997). Briefly, we measured the remanent magnetization of archive-half sections (split cores) with a 2G Enterprises 760R long-core magnetometer (Tables 3–10). Typically, measurements were made every 5 cm prior to and after alternating field (AF) demagnetization. AF demagnetization steps were typically 0, 10, and 20 mT, although occasionally the 10 mT step was skipped owing to time constraints and occasionally 5, 15, or 25 mT demagnetization was used. Never did demagnetization exceed 25 mT because of the limits of the AF coils.

Many of the data from the long-core magnetometer probably contain valid estimates of the characteristic remanence (ChRM) of the sediment. Unfortunately, assessing which intervals are accurate recorders is not easy given the small number of demagnetization steps, the small size of the highest demagnetization step used, the low magnetization of some intervals, coring disturbance, and the ubiquitous presence of a steep downward-directed drill-string overprint.

The overprint is by far the biggest obstacle, though it is probably wholly or at least mostly removed by 10–30 mT demagnetization. This level of demagnetization, however, further reduces the magnetization of the core, with the magnetization of many intervals reaching the resolution of the magnetometer (~2×10^{-4} A/m for a split core). Other intervals apparently do not record a ChRM, the ChRM has been destroyed by diagenesis, and/or the sediments are void of magnetic minerals, in some cases so much so as to be diamagnetic (e.g., Site 1000; Sigurdsson, Leckie, Acton, et al., pp. 251–252, 1997).

We attempted to obtain estimates of the ChRM from the split-core data of the sediments and sedimentary rocks by devising several criteria intended to avoid overprinted or magnetically unstable intervals. Our criteria included (1) rejecting any results below 10-mT demagnetization, (2) rejecting any interval with inclinations steeper than ±60°, a very likely sign that the drill-string overprint is present, (3) rejecting weakly magnetized intervals (<2×10^{-4} A/m), and (4) requiring that directions following two or more AF demagnetization steps of 10 mT or higher from the same interval differ by <3° (a weak analogy to principal component analysis). We also used progressive demagnetization experiments from discrete samples to assess whether an accurate ChRM estimate could be obtained at demagnetization of 10–25 mT (Figs. 2–4). In some cases, obtaining an accurate estimate of the ChRM was difficult even for demagnetization up to 70 mT (Fig. 2). In general, the demagnetization experiments showed that for most intervals 20 mT was marginally sufficient to remove the drill-string overprint (Figs. 3, 4), but in some intervals up to 25–30 mT was required (Fig. 3).

For the split cores from sedimentary units, the number of demagnetization steps completed during Leg 165 were so few that only a few intervals pass the above criteria. Furthermore, demagnetization rarely exceeded 20 mT for the sedimentary cores, which is about the minimum AF field needed to remove the drill-string overprint. Thus, although split-core results for sediments and sedimentary rocks hint at the true ChRM inclinations, significant biases and large uncertainties remain that do not permit their use for paleolatitude estimates. Had the split cores been demagnetized at more steps with higher peak fields (25–70 mT), they very likely could have contributed significant information.

The split-core data from basalt cores, however, provide accurate estimates of the ChRM inclinations for several reasons. Mainly, the results from the basalt cores differ from those from the sedimentary cores because the magnetization of the basalts is much stronger and the overprint is removed by ~10–20 mT, as has been confirmed by the detailed demagnetization of both split-core and discrete samples (e.g., Fig. 5; also see Tables 14, 18). The agreement between the split-core and discrete inclinations from similar intervals, as well as the agreement between split-core inclinations from Holes 1001A and 1001B, are further indication of the quality of the split-core results (Fig. 6).

Because all the basalt cores were demagnetized at 20 mT and most at 25 mT, we have continuous results downcore at demagnetization levels sufficient to resolve the ChRM inclination (Table 15). The continuity of the split-core data is important in that the number of discrete samples collected are, by themselves, insufficient to cover the basalt cores at the same resolution as the split-core data. The higher resolution of the split-core data is particularly useful in assessing the independence of stratigraphically adjacent flow units in sampling geomagnetic SV.

Discrete Samples from Shipboard and Shore-Based Measurements

Discrete samples are either 6-cm^3 cubes collected in 2 cm × 2 cm × 1.5 cm plastic boxes or 8- to 12-cm^3 minicores with a 2.5-cm diameter. These samples were measured at several different laboratories (University of New Mexico, Texas A&M University; Université Pierre et Marie Curie; and on the *JOIDES Resolution* using the Molspin magnetometer during Leg 165 and using a new 2G Enterprises cryogenic magnetometer during Leg 178) and were subjected to a variety of AF and thermal demagnetization treatments (Tables 11–14). For samples that gave linear demagnetization paths on vector demagnetization diagrams, principal component analysis (PCA) (Kirschvink, 1980) was applied to the demagnetization results to determine the ChRM. The Maximum Angular Deviation (MAD) angle, a measure of how well the demagnetization data fit a line, was used to reject samples that gave poorly resolved directions. The MAD angle was required to be <10°, and we generally did not require that the demagnetization paths pass through the origin of the demagnetization plot in the PCA analysis (the "free" option of standard paleomagnetic PCA; Tables 16–18). Only samples with inclinations between +60° and –60° were used. Inclinations steeper than this were rare except in some of the youngest unconsolidated sediments that were weakly magnetized, and, therefore, whose primary magnetizations were likely swamped by the steep drill-string overprint.

Averaging Geomagnetic Secular Variation

Sedimentation rates are lower than 50 m/m.y. (5 cm/k.y.) for Sites 998–1001, typically averaging between 10 and 20 m/m.y. Each sample from a sedimentary unit therefore includes sediments that were deposited over several hundred years to ~2000 yr. To completely average geomagnetic SV, samples spanning a time interval of ~10^5–10^6 yr (more than ~2 m of sedimentary section on average, and <50 m assuming the highest sedimentation rates) are considered sufficient to average SV. The inclination determined from a single sample is thus

Table 1. Flow unit divisions from this study compared with subdivisions used during Leg 165.

Flow unit	Leg 165 unit	Unit Top	Unit Bottom	Depth interval (mbsf)	Leg 165 Formation	Leg 165 Unit	Unit Top	Unit Bottom	Depth interval (mbsf)
53A	4	1001A-52R-8, 30 cm	1001A-53R-4, 43 cm	486.91-491.20					
		1001B-32R-6, 121 cm	1001B-32R-8, 113 cm	486.82-bottom of hole	A	1-4	1001A-52R-6, 59 cm	1001A-53R-4, 43 cm	485.13-491.20
		Chilled margin					Chilled margin		
53B	5	1001A-53R-4, 43 cm	1001A-53R-4, 124 cm	491.20-492.01		5			
	6-10	Basalt breccia, glassy and vesicular rinds			B	6-10	1001A-53R-4, 43 cm	1001A-54R-1, 71 cm	491.20-494.71
54A	11	1001A-54R-1, 0 cm	1001A-54R-1, 71 cm	494.00-494.71		5-11			
	12	Basalt breccia and basaltic hyaloclastite breccia with glassy clastic matrix				12	Basalt breccia, basaltic hyaloclastite breccia, glassy clastic matrix		
54B	13	1001A-54R-2, 24 cm	1001A-54R-2, 105 cm	495.68-496.49		13			
	14-16	Basaltic hyaloclastite breccia with glassy clastic matrix (units 14-16)			C	14-16	1001A-54R-1, 71 cm	1001A-54R-3, 102 cm	494.71-497.89
54C	17	1001A-54R-3, 0 cm	1001A-54R-3, 102 cm	496.87-497.89		12-17			
		Chilled margin					Chilled margin		
54D	18-19	1001A-54R-3, 102 cm	1001A-54R-4, 43 cm	497.89-498.70	D	18-19	1001A-54R-3, 102 cm	1001A-54R-4, 43 cm	497.89-498.70
		Chilled margin					Chilled margin		
54E	20	1001A-54R-4, 43 cm	1001A-54R-4, 127 cm	498.70-499.54		20			
	21	Chilled margin				21	Chilled margin		
54F1	22	1001A-54R-5, 3 cm	1001A-54R-5, 30 cm	499.57-499.84	E	20-22	1001A-54R-4, 43 cm	1001A-54R-5, 30 cm	498.70-499.84
		Chilled margin					Chilled margin		
54F2#	23	1001A-54R-5, 30 cm	1001A-54R-5, 43 cm	499.84-499.97	F	23	1001A-54R-5, 30 cm	1001A-54R-5, 43 cm	499.84-499.97
		Chilled margin and white chalk with possible laminations.					Chilled margin and white chalk with possible laminations.		
54G1	24	1001A-54R-5, 43 cm	1001A-54R-6, 85 cm	499.97-501.89		24			
		Core break with change in basalt texture and an abrupt change in inclination				24			
54G2	24	1001A-54R-6, 85 cm	1001A-54R-7, 40 cm	501.89-502.85		24			
		Glassy basalt possibly a chilled margin			G	24	1001A-54R-5, 43 cm	1001A-54R-7, 85 cm	499.97-503.30
54H	25	1001A-54R-7, 40 cm	1001A-54R-7, 77 cm	502.85-503.22		25			
	26	Carbonate with subangular basalt clasts				24-26			
54I#	27	1001A-54R-7, 85 cm	1001A-54R-7, 107 cm	503.30-503.52	*	27	1001A-54R-7, 85 cm	1001A-54R-7, 107 cm	503.30-503.52
		Basaltic hyaloclastite fragments in a carbonate matrix				28			
55A	29	1001A-55R-1, 3 cm	1001A-55R-1, 105 cm	503.63-504.65	H	28-29	1001A-55R-1, 0 cm	1001A-55R-1, 105 cm	503.60-504.65
		Chilled margin, possibly pillow lava fragments				30-31			
55B	32	1001A-55R-1, 120 cm	1001A-55R-1, 150 cm	504.80-505.10		32			
		Chilled margin, possibly pillow lava fragments				32			
55C	32	1001A-55R-2, 0 cm	1001A-55R-2, 22 cm	505.10-505.32		32			
		Chilled margin, possibly pillow lava fragments				32			
55D	33	1001A-55R-2, 28 cm	1001A-55R-2, 105 cm	505.32-506.15		33			
		Chilled margin				33			
55E	34	1001A-55R-2, 105 cm	1001A-55R-2, 117 cm	506.15-506.27		34			
		Chilled margin			I	34-35	1001A-55R-1, 105 cm	1001A-55R-3, 35 cm	504.65-506.86
55F	35	1001A-55R-2, 121 cm	1001A-55R-2, 140 cm	506.31-506.50		35			
		Chilled margin				36			
55G#	37	1001A-55R-3, 5 cm	1001A-55R-3, 18 cm	506.56-506.69		37			
		Chilled margin				37			
55H	38	1001A-55R-3, 20 cm	1001A-55R-3, 35 cm	506.71-506.86		30-38			
		Chilled margin, many small basalt fragments, possibly pillow fragments				39-45			
55I#	46	1001A-55R-3, 87 cm	1001A-55R-3, 105 cm	507.38-507.56		46			
		Likely recovery gap between cores							
56A	46	1001A-56R-1, 0 cm	1001A-56R-1, 20 cm	513.20-513.40		46			
		Chilled margin			J	47	1001A-55R-3, 35 cm	1001A-56R-1, 78 cm	506.86-513.98
56B	47	1001A-56R-1, 20 cm	1001A-56R-1, 45 cm	513.40-513.65		47			
		Chilled margin				48			
56C#	47	1001A-56R-1, 45 cm	1001A-56R-1, 78 cm	513.65-513.98		39-48			
		Chilled margin with basalt clasts surrounded by calcite matrix				49			
56D	47	1001A-56R-1, 99 cm	1001A-56R-1, 141 cm	514.19-514.61	K	49-50	1001A-56R-1, 78 cm	1001A-56R-1, 141 cm	513.98-514.61
		Chilled margin with basalt clasts surrounded by calcite matrix				51			
56E	52	1001A-56R-2, 67 cm	1001A-56R-3, 99 cm	515.37-517.04	L	52	1001A-56R-1, 141 cm	1001A-56R-3, 137 cm	514.61-517.42

Notes: Leg 165 Unit gives the unit names and Leg 165 Formation gives the formation names from Sigurdsson, Leckie, Acton, et al. (1997). Chilled margins are evidenced by quench basalts typically with glass. # = no reliable paleomagnetic data were obtained from these units; * = not included in any formation.

Table 2. List of data tables stored on the CD-ROM in the back pocket of this volume.

Table	Title
3	Split-core (archive half) paleomagnetic data from Hole 998A.
4	Split-core (archive half) paleomagnetic data from Hole 998B.
5	Split-core (archive half) paleomagnetic data from Hole 999A.
6	Split-core (archive half) paleomagnetic data from Hole 999B.
7	Split-core (archive half) paleomagnetic data from Hole 1000A.
8	Split-core (archive half) paleomagnetic data from Hole 1000B.
9	Split-core (archive half) paleomagnetic data from Hole 1001A.
10	Split-core (archive half) paleomagnetic data from Hole 1001B.
11	Paleomagnetic data from discrete samples from Site 998.
12	Paleomagnetic data from discrete samples from Site 999.
13	Paleomagnetic data from discrete samples from Site 1000.
14	Paleomagnetic data from discrete samples from Site 1001.
15	Basalt split-core inclinations after AF demagnetization and after removing data from near the ends of core sections and coring gaps.
16	Inclinations from principal component analysis of discrete samples from Site 998.
17	Inclinations from principal component analysis of discrete samples from Site 999.
18	Inclinations from principal component analysis of discrete samples from Site 1001.

Table 3. Split-core (archive half) paleomagnetic data from Hole 998A obtained during Leg 165.

Sample ID	Interval (cm)	Depth (mbsf)	Demag step (mT)	Declination (°)	Inclination (°)	Intensity (A/m)
165-998A-001H-01	5	0.05	0	277.1	45.6	3.83E-03
165-998A-001H-01	5	0.05	10	298.2	69.8	2.07E-03
165-998A-001H-01	5	0.05	15	350.1	77.2	1.89E-03
165-998A-001H-01	15	0.15	0	281.4	49.0	1.82E-02
165-998A-001H-01	15	0.15	10	288.1	53.8	1.21E-02
165-998A-001H-01	15	0.15	15	289.9	60.5	9.49E-03
165-998A-001H-01	25	0.25	0	276.8	58.4	2.25E-02
165-998A-001H-01	25	0.25	10	281.0	65.3	1.34E-02
165-998A-001H-01	25	0.25	15	292.1	70.2	1.07E-02
165-998A-001H-01	35	0.35	0	301.3	58.5	2.32E-02

This is a sample of the table that appears on the volume CD-ROM.

Table 4. Split-core (archive half) paleomagnetic data from Hole 998B obtained during Leg 165.

Sample ID	Interval (cm)	Depth (mbsf)	Demag Step (mT)	Declination (°)	Inclination (°)	Intensity (A/m)
165-998B-001R-01	5	558.35	0	197.6	22.5	3.49E-04
165-998B-001R-01	5	558.35	10	215.6	–10.3	1.03E-04
165-998B-001R-01	5	558.35	15	182.2	–31.6	1.25E-04
165-998B-001R-01	5	558.35	20	179.4	–10.1	2.44E-04
165-998B-001R-01	15	558.45	0	174.5	–5.2	3.16E-04
165-998B-001R-01	15	558.45	10	162.3	–46.3	2.37E-04
165-998B-001R-01	15	558.45	15	167.8	–39.6	3.03E-04
165-998B-001R-01	15	558.45	20	117.6	–73.3	1.91E-04
165-998B-001R-01	25	558.55	0	167.1	1.3	3.72E-04
165-998B-001R-01	25	558.55	10	159.1	–39.3	2.95E-04

This is a sample of the table that appears on the volume CD-ROM.

Table 5. Split-core (archive half) paleomagnetic data from Hole 999A obtained during Leg 165.

Sample ID	Interval (cm)	Depth (mbsf)	Demag Step (mT)	Declination (°)	Inclination (°)	Intensity (A/m)
165-999A-001H-03	5	3.05	0	357.5	51.4	2.12E-02
165-999A-001H-03	5	3.05	10	355.3	–2.7	3.68E-03
165-999A-001H-03	5	3.05	20	352.7	–8.7	2.14E-03
165-999A-001H-03	15	3.15	0	354.7	60.4	2.43E-02
165-999A-001H-03	15	3.15	10	356.4	–2.7	3.61E-03
165-999A-001H-03	15	3.15	20	354.8	–13.6	1.71E-03
165-999A-001H-03	25	3.25	0	354.9	58.5	2.46E-02
165-999A-001H-03	25	3.25	10	358.3	0.4	4.29E-03
165-999A-001H-03	25	3.25	20	358.6	–6.8	2.14E-03
165-999A-001H-03	35	3.35	0	349.0	57.6	2.63E-02

This is a sample of the table that appears on the volume CD-ROM.

Table 6. Split-core (archive half) paleomagnetic data from Hole 999B obtained during Leg 165.

Sample ID	Interval (cm)	Depth (mbsf)	Demag Step (mT)	Declination (°)	Inclination (°)	Intensity (A/m)
165-999B-005R-01	5	572.65	0	52.1	47.4	5.47E-03
165-999B-005R-01	5	572.65	10	79.8	13.9	3.05E-03
165-999B-005R-01	5	572.65	20	81.6	9.9	1.92E-03
165-999B-005R-01	15	572.75	0	31.6	64.8	7.87E-03
165-999B-005R-01	15	572.75	10	64.1	34.2	2.01E-03
165-999B-005R-01	15	572.75	20	72.3	27.0	1.11E-03
165-999B-005R-01	25	572.85	0	38.4	71.0	8.15E-03
165-999B-005R-01	25	572.85	10	64.6	45.5	2.15E-03
165-999B-005R-01	25	572.85	20	50.9	36.4	1.31E-03
165-999B-005R-01	35	572.95	0	17.9	58.5	8.60E-03

This is a sample of the table that appears on the volume CD-ROM.

Table 7. Split-core (archive half) paleomagnetic data from Hole 1000A obtained during Leg 165.

Sample ID	Interval (cm)	Depth (mbsf)	Demag Step (mT)	Declination (°)	Inclination (°)	Intensity (A/m)
165-1000A-001H-01	5	0.05	0	290.0	28.7	4.31E-02
165-1000A-001H-01	5	0.05	10	345.9	–2.2	3.31E-03
165-1000A-001H-01	5	0.05	20	343.6	–7.8	2.78E-03
165-1000A-001H-01	15	0.15	0	221.2	73.2	5.40E-02
165-1000A-001H-01	15	0.15	10	23.3	14.6	8.56E-03
165-1000A-001H-01	15	0.15	20	18.0	8.8	7.71E-03
165-1000A-001H-01	25	0.25	0	52.4	62.5	2.02E-02
165-1000A-001H-01	25	0.25	10	91.5	–7.1	5.63E-03
165-1000A-001H-01	25	0.25	20	90.3	–13.6	4.71E-03
165-1000A-001H-01	35	0.35	0	75.2	76.5	2.18E-02

This is a sample of the table that appears on the volume CD-ROM.

Table 8. Split-core (archive half) paleomagnetic data from Hole 1000B obtained during Leg 165.

Sample ID	Interval (cm)	Depth (mbsf)	Demag Step (mT)	Declination (°)	Inclination (°)	Intensity (A/m)
165-1000B-001R-01	5	79.35	0	261.3	–4.2	1.79E-02
165-1000B-001R-01	5	79.35	20	38.5	46.7	5.46E-04
165-1000B-001R-01	15	79.45	0	87.7	4.2	4.58E-03
165-1000B-001R-01	15	79.45	20	357.5	14.6	4.85E-04
165-1000B-001R-01	25	79.55	0	34.6	46.9	5.46E-04
165-1000B-001R-01	25	79.55	20	4.7	11.5	4.01E-04
165-1000B-001R-01	35	79.65	0	62.5	12.7	4.52E-04
165-1000B-001R-01	35	79.65	20	5.6	17.2	4.97E-04
165-1000B-001R-01	45	79.75	0	285.2	–14.1	1.05E-03
165-1000B-001R-01	45	79.75	20	1.5	19.8	4.81E-04

This is a sample of the table that appears on the volume CD-ROM.

Table 9. Split-core (archive half) paleomagnetic data from Hole 1001A obtained during Leg 165.

Sample ID	Interval (cm)	Depth (mbsf)	Demag Step (mT)	Declination (°)	Inclination (°)	Intensity (A/m)
165-1001A-002R-01	5	6.45	0	310.6	74.3	1.54E-02
165-1001A-002R-01	5	6.45	10	333.8	72.4	1.22E-02
165-1001A-002R-01	5	6.45	15	337.7	72.7	1.06E-02
165-1001A-002R-01	5	6.45	20	340.2	72.5	8.87E-03
165-1001A-002R-01	15	6.55	0	110.6	83.4	2.09E-02
165-1001A-002R-01	15	6.55	10	82.7	81.6	1.69E-02
165-1001A-002R-01	15	6.55	15	79.6	81.4	1.47E-02
165-1001A-002R-01	15	6.55	20	80.4	81.3	1.23E-02
165-1001A-002R-01	25	6.65	0	244.3	86.6	1.99E-02
165-1001A-002R-01	25	6.65	10	284.7	83.9	1.65E-02

This is a sample of the table that appears on the volume CD-ROM.

Table 10. Split-core (archive half) paleomagnetic data from Hole 1001B obtained during Leg 165.

Sample ID	Interval (cm)	Depth (mbsf)	Demag Step (mT)	Declination (°)	Inclination (°)	Intensity (A/m)
165-1001B-001R-01	5	25.35	0	332.2	–1.7	5.17E-02
165-1001B-001R-01	5	25.35	10	355.2	54.8	1.25E-02
165-1001B-001R-01	5	25.35	20	60.5	70.9	9.16E-03
165-1001B-001R-01	15	25.45	0	209.5	41.3	9.03E-02
165-1001B-001R-01	15	25.45	10	257.9	78.7	3.06E-02
165-1001B-001R-01	15	25.45	20	2.2	80.4	2.17E-02
165-1001B-001R-01	25	25.55	0	152.6	31.2	1.08E-01
165-1001B-001R-01	25	25.55	10	141.2	79.1	3.34E-02
165-1001B-001R-01	25	25.55	20	344.3	80.9	2.34E-02
165-1001B-001R-01	35	25.65	0	5.2	60.2	4.19E-02

This is a sample of the table that appears on the volume CD-ROM.

Table 11. Paleomagnetic results from discrete samples from Site 998.

Sample ID	Interval (cm)	Depth (mbsf)	Step (#)	Type	Demag Step	Declination (°)	Inclination (°)	Intensity (A/m)	Laboratory
165-0998A-001H-01	61.0	0.61	1	N	0	45.7	65.2	9.902E-03	ODP_JRMM_LAB
165-0998A-001H-01	61.0	0.61	2	H	10	40.7	59.2	6.115E-03	ODP_JRMM_LAB
165-0998A-001H-01	61.0	0.61	3	H	20	35.7	58.2	4.062E-03	ODP_JRMM_LAB
165-0998A-001H-01	61.0	0.61	4	H	30	34.0	57.3	4.864E-03	ODP_JRMM_LAB
165-0998A-001H-01	61.0	0.61	5	H	40	30.4	58.6	3.408E-03	ODP_JRMM_LAB
165-0998A-001H-01	61.0	0.61	6	H	50	26.2	52.8	2.836E-03	ODP_JRMM_LAB
165-0998A-001H-01	61.0	0.61	7	H	60	5.0	47.1	2.088E-03	ODP_JRMM_LAB
165-0998A-001H-02	61.0	2.11	1	N	0	28.5	71.2	4.621E-03	ODP_JRMM_LAB
165-0998A-001H-02	61.0	2.11	2	H	10	31.6	71.4	3.793E-03	ODP_JRMM_LAB
165-0998A-001H-02	61.0	2.11	3	H	20	31.4	71.4	2.806E-03	ODP_JRMM_LAB

Notes: Site latitude = 19.490°N, longitude = 277.064°E; all samples are from the working halves of the split cores. Sample volume = 6 cm^3; Sample ID = the leg, site, hole, core, core type, and section following standard ODP naming conventions; Step (#) = the order in which the demagnetization steps were conducted; Demag Type = the type of demagnetization treatment used, where N = no demagnetization, H = alternating field, and T = thermal. Demag Step = the size of peak AF demagnetization field (mT) or the temperature (°C) of the oven during the demagnetization step. Laboratory sample analyses were conducted in several laboratories as given by the following codes: ODP_JRMM_LAB = shipboard measurements made on the *JOIDES Resolution* during Leg 165 using the Molspin Magnetometer; ODP_JRAC_LAB = shipboard measurements made on the *JOIDES Resolution* during Leg 165 using the AC-SQUID Cryogenic Magnetometer; ODP_JRDC_LAB = shipboard measurements made on the *JOIDES Resolution* during Leg 178 using the DC-SQUID Cryogenic Magnetometer; UNM_AC_LAB = shore-based measurements made at the University of New Mexico using an AC-SQUID Cryogenic Magnetometer; ODP_TAMU_LAB = shore-based measurements made at Texas A&M University using an AC-SQUID Cryogenic Magnetometer; UNM+JRMM_LAB = initial measurements made on the *JOIDES Resolution* during Leg 165 using the Molspin Magnetometer with additional measurements made at higher demagnetization steps at the University of New Mexico using an AC-SQUID Cryogenic Magnetometer.

This is a sample of the table that appears on the volume CD-ROM.

Table 12. Paleomagnetic results from discrete samples from Site 999.

Sample ID	Interval (cm)	Depth (mbsf)	Step (#)	Type	Demag step	Declination (°)	Inclination (°)	Intensity (A/m)	Laboratory
165-0999A-001H-01	63	0.63	1	N	0	0	39.1	9.10E-05	ODP_JRAC_LAB
165-0999A-001H-01	63	0.63	2	H	10	11.5	32.9	7.37E-04	ODP_JRAC_LAB
165-0999A-001H-01	63	0.63	3	H	20	26.6	28.8	5.83E-04	ODP_JRAC_LAB
165-0999A-001H-01	63	0.63	4	H	40	7.8	24.8	2.83E-04	ODP_JRAC_LAB
165-0999A-001H-01	63	0.63	5	H	60	0	22.8	1.81E-04	ODP_JRAC_LAB
165-0999A-001H-02	63	2.13	1	N	0	3.2	47.2	4.67E-04	ODP_JRAC_LAB
165-0999A-001H-02	63	2.13	2	H	10	2.5	25.0	4.47E-04	ODP_JRAC_LAB
165-0999A-001H-02	63	2.13	3	H	20	10.9	23.9	3.04E-04	ODP_JRAC_LAB
165-0999A-001H-02	63	2.13	4	H	40	350.0	26.2	1.69E-04	ODP_JRAC_LAB
165-0999A-001H-02	63	2.13	5	H	60	0	26.6	4.90E-05	ODP_JRAC_LAB

Notes: Site latitude = 12.74°N, longitude = 281.26°E; all samples are from the working halves of the split cores. Sample volume = 6 cm^3; Sample ID = the leg, site, hole, core, core type, and section following standard ODP naming conventions; Step (#) = the order in which the demagnetization steps were conducted; Demag Type = the type of demagnetization treatment used, where N = no demagnetization, H = alternating field, and T = thermal. Demag Step = the size of peak AF demagnetization field (mT) or the temperature (°C) of the oven during the demagnetization step. Laboratory sample analyses were conducted in several laboratories as given by the following codes: ODP_JRMM_LAB = shipboard measurements made on the *JOIDES Resolution* during Leg 165 using the Molspin Magnetometer; ODP_JRAC_LAB = shipboard measurements made on the *JOIDES Resolution* during Leg 165 using the AC-SQUID Cryogenic Magnetometer; ODP_JRDC_LAB = shipboard measurements made on the *JOIDES Resolution* during Leg 178 using the DC-SQUID Cryogenic Magnetometer; UNM_AC_LAB = shore-based measurements made at the University of New Mexico using an AC-SQUID Cryogenic Magnetometer; ODP_TAMU_LAB = shore-based measurements made at Texas A&M University using an AC-SQUID Cryogenic Magnetometer; UNM+JRMM_LAB = initial measurements made on the *JOIDES Resolution* during Leg 165 using the Molspin Magnetometer with additional measurements made at higher demagnetization steps at the University of New Mexico using an AC-SQUID Cryogenic Magnetometer.

This is a sample of the table that appears on the volume CD-ROM.

Table 13. Paleomagnetic results from discrete samples from Site 1000.

Sample ID	Interval (cm)	Depth (mbsf)	Step (#)	Type	Demag Step	Declination (°)	Inclination (°)	Intensity (A/m)	Laboratory
165-1000A-001H-01	120	1.2	1	N	0	193.9	15.0	5.77E-04	ODP-JRDC-LAB
165-1000A-001H-01	120	1.2	2	H	5	206.9	28.8	4.33E-04	ODP-JRDC-LAB
165-1000A-001H-01	120	1.2	3	H	10	219.1	41.7	4.43E-04	ODP-JRDC-LAB
165-1000A-001H-01	120	1.2	4	H	15	219.3	28.4	4.84E-04	ODP-JRDC-LAB
165-1000A-001H-01	120	1.2	5	H	20	213.0	16.2	4.80E-04	ODP-JRDC-LAB
165-1000A-001H-01	120	1.2	6	H	25	217.3	22.9	5.43E-04	ODP-JRDC-LAB
165-1000A-001H-01	120	1.2	7	H	30	221.5	4.3	3.90E-04	ODP-JRDC-LAB
165-1000A-001H-01	120	1.2	8	H	35	228.4	15.2	4.91E-04	ODP-JRDC-LAB
165-1000A-001H-01	120	1.2	9	H	40	232.4	16.1	5.49E-04	ODP-JRDC-LAB
165-1000A-001H-01	120	1.2	10	H	50	205.6	–24.2	6.92E-04	ODP-JRDC-LAB

Notes: Site latitude = 16.55°N, longitude = 280.13°E; all samples are from the working halves of the split cores. Sample volume = 6 cm^3; Sample ID = the leg, site, hole, core, core type, and section following standard ODP naming conventions; Step (#) = the order in which the demagnetization steps were conducted; Demag Type = the type of demagnetization treatment used, where N = no demagnetization, H = alternating field, and T = thermal. Demag Step = the size of peak AF demagnetization field (mT) or the temperature (°C) of the oven during the demagnetization step. Laboratory sample analyses were conducted in several laboratories as given by the following codes: ODP_JRMM_LAB = shipboard measurements made on the *JOIDES Resolution* during Leg 165 using the Molspin Magnetometer; ODP_JRAC_LAB = shipboard measurements made on the *JOIDES Resolution* during Leg 165 using the AC-SQUID Cryogenic Magnetometer; ODP_JRDC_LAB = shipboard measurements made on the *JOIDES Resolution* during Leg 178 using the DC-SQUID Cryogenic Magnetometer; UNM_AC_LAB = shore-based measurements made at the University of New Mexico using an AC-SQUID Cryogenic Magnetometer; ODP_TAMU_LAB = shore-based measurements made at Texas A&M University using an AC-SQUID Cryogenic Magnetometer; UNM+JRMM_LAB = initial measurments made on the *JOIDES Resolution* during Leg 165 using the Molspin Magnetometer with additional measurements made at higher demagnetization steps at the University of New Mexico using an AC-SQUID Cryogenic Magnetometer.

This is a sample of the table that appears on the volume CD-ROM.

Table 14. Paleomagnetic results from discrete samples from Site 1001.

Sample ID	Interval (cm)	Depth (mbsf)	Step (#)	Type	Demag step	Declination (°)	Inclination (°)	Intensity (A/m)	Laboratory
165-1001A-002R-01	17	6.57	1	N	0	137.1	64.5	8.13E-03	UNM___AC_LAB
165-1001A-002R-01	17	6.57	2	H	10	136.3	64.5	7.14E-03	UNM___AC_LAB
165-1001A-002R-01	17	6.57	3	H	20	133.0	65.8	5.97E-03	UNM___AC_LAB
165-1001A-002R-01	17	6.57	4	H	30	132.7	65.0	4.76E-03	UNM___AC_LAB
165-1001A-002R-01	17	6.57	5	H	40	134.8	64.2	3.71E-03	UNM___AC_LAB
165-1001A-002R-01	17	6.57	6	H	50	139.2	62.7	2.84E-03	UNM___AC_LAB
165-1001A-002R-01	17	6.57	7	H	60	142.2	61.3	2.20E-03	UNM___AC_LAB
165-1001A-002R-01	17	6.57	8	H	70	143.1	60.6	1.75E-03	UNM___AC_LAB
165-1001A-002R-01	17	6.57	9	H	85	136.1	66.0	1.07E-03	UNM___AC_LAB
165-1001A-002R-01	17	6.57	10	H	100	159.2	59.8	7.15E-04	UNM___AC_LAB

Notes: Site latitude = 15.76°N, longitude = 285.09°E; all samples are from the working halves of the split cores. Sample volume = 6 cm^3; Sample ID = the leg, site, hole, core, core type, and section following standard ODP naming conventions; Step (#) = the order in which the demagnetization steps were conducted; Demag Type = the type of demagnetization treatment used, where N = no demagnetization, H = alternating field, and T = thermal. Demag Step = the size of peak AF demagnetization field (mT) or the temperature (°C) of the oven during the demagnetization step. Laboratory sample analyses were conducted in several laboratories as given by the following codes: ODP_JRMM_LAB = shipboard measurements made on the *JOIDES Resolution* during Leg 165 using the Molspin Magnetometer; ODP_JRAC_LAB = shipboard measurements made on the *JOIDES Resolution* during Leg 165 using the AC-SQUID Cryogenic Magnetometer; ODP_JRDC_LAB = shipboard measurements made on the *JOIDES Resolution* during Leg 178 using the DC-SQUID Cryogenic Magnetometer; UNM_AC_LAB = shore-based measurements made at the University of New Mexico using an AC-SQUID Cryogenic Magnetometer; ODP_TAMU_LAB = shore-based measurements made at Texas A&M University using an AC-SQUID Cryogenic Magnetometer; UNM+JRMM_LAB = initial measurments made on the *JOIDES Resolution* during Leg 165 using the Molspin Magnetometer with additional measurements made at higher demagnetization steps at the University of New Mexico using an AC-SQUID Cryogenic Magnetometer.

This is a sample of the table that appears on the volume CD-ROM.

Table 15. Basalt split-core inclinations after AF demagnetization and after removing data from near the ends of core sections and coring gaps.

Leg	Site	Hole	Core	Core type	Section	Interval (cm)	Depth (mbsf)	AF demag (mT)	Inclination (°)	Intensity (mA/m)
Flow unit 53A										
165	1001	B	32	R	7	45	487.56	25	24.00	3.822E+01
165	1001	B	32	R	7	55	487.66	25	21.00	8.104E+01
165	1001	B	32	R	7	65	487.76	25	34.50	5.975E+01
165	1001	B	32	R	7	75	487.86	25	19.00	1.665E+02
165	1001	B	32	R	7	85	487.96	25	16.60	7.254E+01
165	1001	B	32	R	8	10	488.22	25	17.30	1.657E+02
165	1001	B	32	R	8	15	488.27	25	19.50	1.471E+02
165	1001	B	32	R	8	20	488.32	25	21.70	1.147E+02
165	1001	B	32	R	8	25	488.37	25	26.00	7.940E+01
165	1001	B	32	R	8	30	488.42	25	27.30	7.276E+01

Note: Data are divided into flow units as defined in Table 1.

This is a sample of the table that appears on the volume CD-ROM.

Table 16. Inclinations from principal component analysis of discrete samples from ODP Site 998.

Sample ID	Depth (mbsf)	Inclination (°)	MAD	Type	Paleolatitude
165-0998A-001H-5, 61 cm	6.61	37.70	2.88	FRE	21.13
165-0998A-001H-6, 61 cm	8.11	48.70	5.44	FRE	29.65
165-0998A-002H-2, 61 cm	10.91	55.40	7.41	FRE	35.93
165-0998A-002H-4, 11 cm	13.41	38.10	9.28	FRE	21.41
165-0998A-002H-4, 61 cm	13.91	46.70	9.32	FRE	27.95
165-0998A-002H-5, 61 cm	15.41	37.70	6.98	FRE	21.13
165-0998A-002H-6, 61 cm	16.91	28.90	7.71	FRE	15.43
165-0998A-003H-5, 61 cm	24.91	30.10	9.37	FRE	16.16
165-0998A-004H-5, 61 cm	34.41	–21.90	4.43	FRE	11.36
165-0998A-008H-3, 61 cm	69.41	21.90	1.78	FRE	11.36

Notes: Inclinations are estimated from principal component inclination analysis (PCA). MAD = maximum angular deviation from the demagnetization data in the PCA (Kirschvink, 1980). Type = description of the type of line fitted through the demagnetization data in the PCA, where FRE = a line fit through the data only, ANC = a line fit through the data, but anchored to the origin of the demagnetization plot, and BRU = PCA results provided by Bruno Galbrun, used by V. Louvel and B. Galbrun (unpubl. data).

This is a sample of the table that appears on the volume CD-ROM.

Table 17. Inclinations from principal component analysis of discrete samples from ODP Site 999.

Sample ID	Depth (mbsf)	Inclination (°)	MAD	Type	Paleolatitude
165-0999A-001H-2, 63 cm	2.13	24.30	9.39	FRE	12.72
165-0999A-001H-3, 63 cm	3.63	19.10	7.47	FRE	9.82
165-0999A-001H-5, 63 cm	6.63	21.70	9.71	FRE	11.25
165-0999A-003H-4, 63 cm	22.23	25.10	5.11	FRE	13.18
165-0999A-003H-5, 3 cm	23.13	19.90	3.48	FRE	10.26
165-0999A-004H-3, 63 cm	30.23	–13.90	8.90	ANC	6.90
165-0999A-004H-4, 63 cm	31.73	–24.90	1.44	FRE	13.07
165-0999A-004H-5, 63 cm	33.23	–39.30	1.23	FRE	22.26
165-0999A-004H-6, 63 cm	34.73	–36.40	5.11	FRE	20.24
165-0999A-004H-7, 63 cm	36.23	39.90	5.02	FRE	22.69

Notes: Inclinations are estimated from principal component analysis (PCA); MAD = maximum angular deviation from the principal component analysis (Kirschvink, 1980); Type = description of the type of line fitted through the demagnetization data in the PCA, where FRE = a line fit through the data only, ANC = a line fit through the data, but anchored to the origin of the demagnetization plot, and BRU = PCA results provided by Bruno Galbrun, used by V. Louvel and B. Galbrun (unpubl. data).

This is a sample of the table that appears on the volume CD-ROM.

Table 18. Inclinations from principal component analysis of discrete samples from ODP Site 1001.

Sample ID	Depth (mbsf)	Inclination (°)	MAD	Type	Paleolatitude
Sedimentary samples					
165-1001A-018R-1, 14 cm	160.43	42.00	9.99	BRU	24.24
165-1001A-018R-2, 17 cm	161.96	40.50	9.99	BRU	23.12
165-1001A-018R-3, 19 cm	163.48	–3.60	9.99	BRU	1.80
165-1001A-018R-4, 63 cm	165.42	–1.00	9.99	BRU	0.50
165-1001A-020R-1, 54 cm	170.53	–2.70	9.99	BRU	1.35
165-1001A-021R-1, 42 cm	180.01	–9.70	9.99	BRU	4.89
165-1001A-023R-1, 85 cm	199.64	15.20	9.99	BRU	7.74
165-1001A-024R-1, 46 cm	208.85	–4.50	9.99	BRU	2.25
165-1001A-024R-1, 82 cm	209.22	–14.30	4.30	ANC	7.26
165-1001A-024R-2, 21 cm	210.10	3.60	9.99	BRU	1.80

Notes: Inclinations are estimated from principal component analysis (PCA); MAD = maximum angular deviation from the principal component analysis (Kirschvink, 1980); Type = description of the type of line fitted through the demagnetization data in the PCA, where FRE = a line fit through the data only, ANC = a line fit through the data, but anchored to the origin of the demagnetization plot, and BRU = PCA results provided by Bruno Galbrun, used by V. Louvel and B. Galbrun (unpubl. data).

This is a sample of the table that appears on the volume CD-ROM.

representative of a partially time-averaged geomagnetic field. To ensure that SV is fully averaged along with other sources of noise, we compute mean paleolatitudes from groups of samples that span 50–100 m of drilling depth. The best estimates come from correcting this mean for a bias that arises because the geomagnetic polarity of azimuthally unoriented drill cores is unknown in some cases. We refer to this as the polarity ambiguity (POAM) bias (described below).

Basalt samples from a single flow only give an instantaneous measure of the geomagnetic field. In some cases, multiple flows may be extruded within such a short time interval that they only provide redundant samples of the same instant of geomagnetic field variation. To average SV, generally more than ~10 independent samples of the field are considered sufficient. As shown below, the 30 m of basalts probably contain ~12 independent units. The best estimate of the paleolatitude from the basaltic basement comes from the mean of these 12 independent units, after correcting for the POAM bias (Tables 19–21).

Calculating Mean Paleolatitudes

We group the paleomagnetic inclinations by depth within each hole and then compute the mean paleolatitude for each depth range in two ways (Table 21). In the first method (column labeled “A-Mean Paleolatitude” in Table 21), we take the absolute value of inclinations

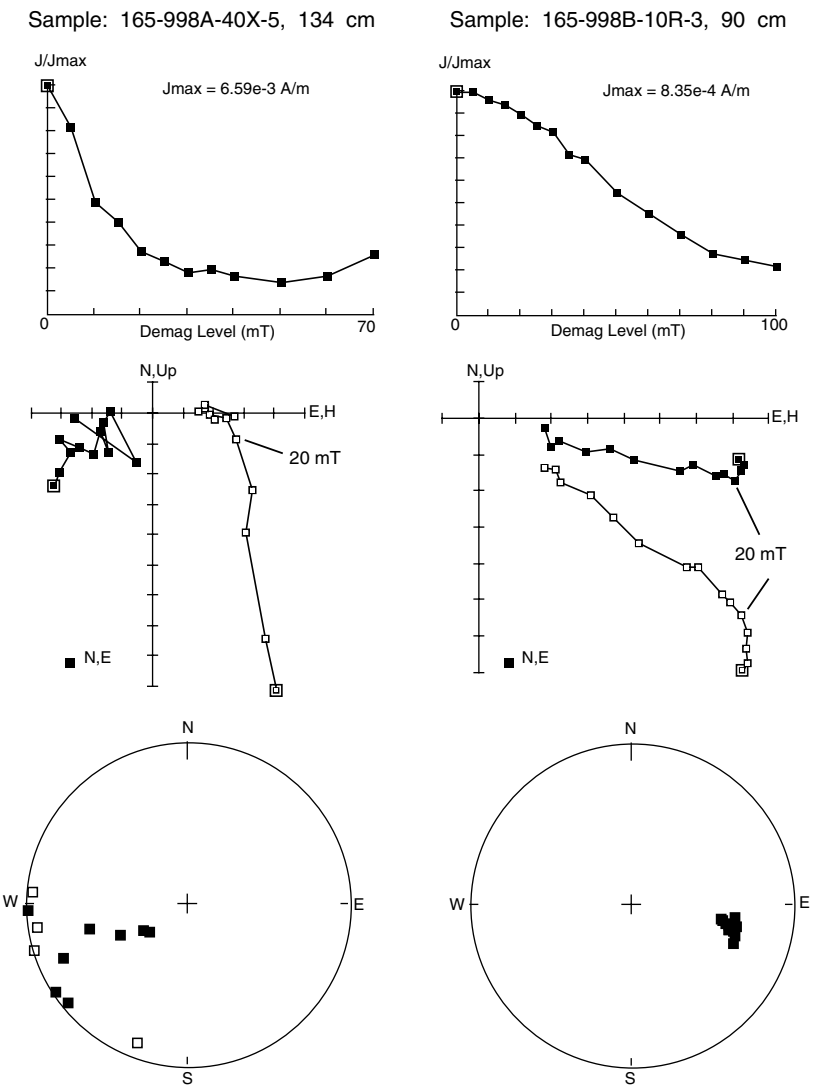

Figure 2. AF demagnetization results for Samples 165-998A-40X-5, 134 cm, and 165-998B-10R-3, 90 cm. Top diagrams show the intensity variation with progressive demagnetization; the middle diagrams show vector end points on a vector demagnetization diagram (orthogonal projections where open squares are inclination and solid squares are declination); and the bottom diagrams show the magnetization directions on equal-area stereonets (open squares are directions with negative inclinations). As is typical for many samples from Site 998, these samples have a steep drill-string overprint. Demagnetization removes the overprint, but often all that remains is a poorly defined ChRM, as is the case for Sample 165-998A-40X-5, 134 cm. Less often, stable ChRM directions can be defined as shown for Sample 165-998B-10R-3, 90 cm. J/Jmax = intensity (J) normalized by the maximum intensity (Jmax) measured during demagnetization.

for a group of samples, convert these to paleolatitudes, and then compute the mean. For example, there are 33 samples from 848 to 903 mbsf from Hole 998B, 16 with positive and 17 with negative inclinations. The mean paleolatitude from all 33 samples is 8.5°. In the second method (column labeled "B-Mean Paleolatitude" in Table 21), we find the mean paleolatitude from all the samples with positive inclinations and the mean paleolatitude from the absolute value of all the samples with negative inclinations, and then average these two values. For the example from Hole 998B, the mean computed this way is 8.6°.

These "B-Mean" paleolatitudes are useful for assessing the effect of possible unremoved secondary components. Again, we use the 33 samples from 848 to 903 mbsf from Hole 998B as an example case. Comparison of the mean inclination of the samples with positive inclinations (21.9°) to the mean of those with negative inclinations (–10.7°), indicates that the drill-string overprint seen in the split-core results is probably also present in the discrete samples. The effect is what would be expected if a present-day and/or a drill-string overprint were present (i.e., the normal polarity directions would be biased toward steeper directions and the reversed polarity directions toward shallower). Assuming this overprint is present, then the size of the bias produced by the overprint, which can be estimated from the means, is ~5.6° [= (21.9° – 10.7°)/2] of inclination or ~2°–3° of paleolatitude. Because there are roughly equal numbers of samples with positive and negative inclinations, the bias is also canceled when the "A-Mean" paleolatitude is computed. If all the samples had the same sign, then the mean paleolatitude computed from them may have been biased by a few degrees.

In general, the means computed either way differ little because within each group there are similar numbers of samples with positive and negative inclinations. As discussed further below, because the sign of the inclination is not always indicative of the polarity of the sample, using the "B-Mean" paleolatitude may result in other biases. Also, using the "B-Mean" assumes that differences between the means of positive- and negative-inclination groups are related to secondary overprints rather than to a primary signal, which may not always be the case. We compute the "B-Mean" here only to illustrate the sense and size of possible secondary overprints on the paleolatitude estimates. On average, the "B-Mean" paleolatitude is only 0.6° less than the "A-Mean," and therefore, the effect of the overprint, if present, is negligible.

Our preferred mean paleolatitudes are the "A-Mean" paleolatitudes corrected for the POAM bias as discussed below.

Estimating Paleolatitudes from Azimuthally Unoriented Drill Cores with Shallow Inclinations

Estimating paleolatitudes from inclination data requires care as all estimators are biased and corrections need to be applied (Briden and Ward, 1966; Kono, 1980; McFadden and Reid, 1982; Cox and Gor-

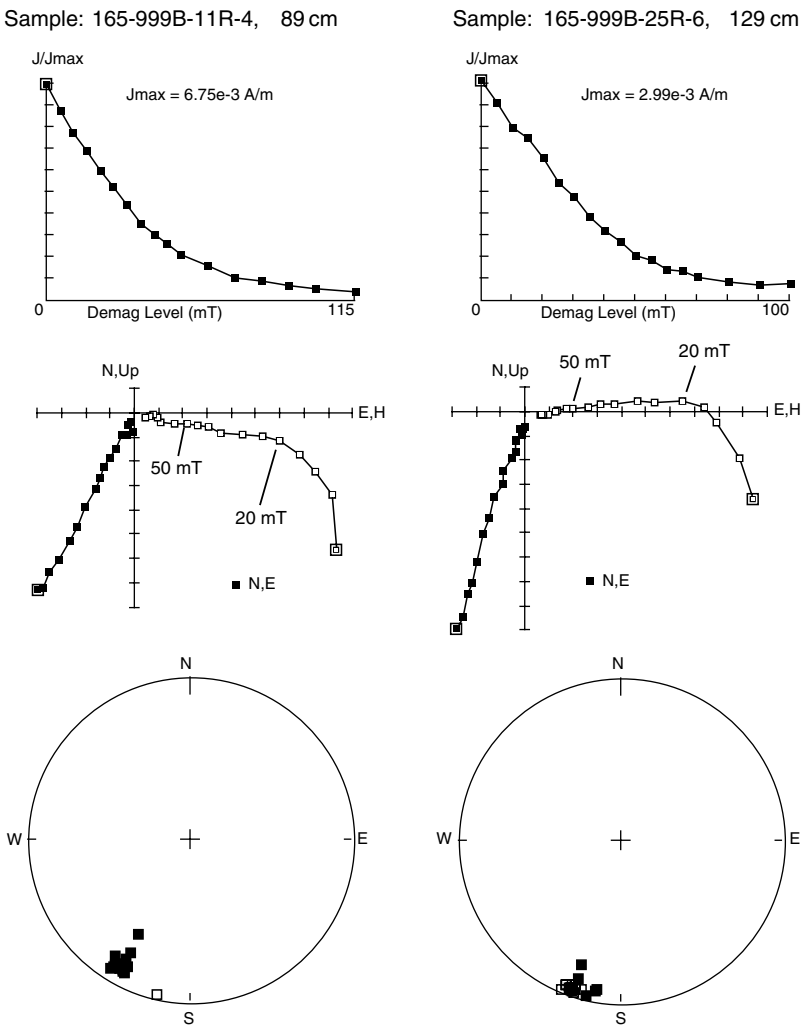

Figure 3. AF demagnetization results from Site 999 for sedimentary Samples 165-999B-11R-4, 89 cm (~25 Ma), and 165-999B-25R-6, 129 cm (~34 Ma). Note the steep downward-directed overprint that is removed by ~20 mT, leaving shallow ChRM directions. See Figure 2 caption for diagram descriptions.

don, 1984). The bias can be easily visualized for the case where the paleomagnetic pole and site lie at the same geographic point (i.e., the angular distance between the pole and the site, called the colatitude, is 0°). Consider a Fisherian distributed set of paleomagnetic poles about this mean. The angular distance between each of these poles and the mean pole gives a colatitude estimate, which will nearly always be >0°. We refer to this bias as the angular distance (AD) bias. The effect of the AD bias for paleolatitude studies is such that the mean, median, or other estimators of the colatitude will naturally be greater than the true colatitude of 0°. As discussed by Cox and Gordon (1984), the size of the bias (1) is large (comparable to the angular standard deviation of the observed colatitudes, which will be >8° for most paleomagnetic data sets) when the true paleolatitude is within a few degrees of the geographic poles; (2) is several degrees or more for latitudes >50°; (3) is less than ~0.5° within 25° of latitude of the equator; and (4) decreases to zero at the equator.

Thus, when analyzing inclination only data sets with shallow inclinations, the AD bias apparently should be very small or negligible. This generally is the case for the sedimentary units sampled here because the dispersion caused by SV is small and the Caribbean plate has been within 25° of the equator. The AD bias would likewise appear to be negligible for the basalt samples because they too must have formed within ~25° of the equator. This assumes, however, that the geomagnetic polarity of the rock sample from which the inclination was obtained is known, or at least that all rock samples have the same polarity.

For azimuthally unoriented drill cores from rock units that formed near the equator, determining the polarity of sedimentary units may be difficult and determining the polarity of basalt units nearly impossible. The polarity ambiguity arises for several reasons: (1) Because the cores are azimuthally unoriented, the declination cannot be used to determine polarity. (2) Because the inclination is shallow at or near the equator, the angular distance between reversed and normal polarity inclinations is small. (3) Because the paleomagnetic inclinations from any suite of rocks will have some degree of dispersion about their mean inclination, it is likely that when the mean inclination is shallow, the sign of the inclination will not be indicative of the polarity. This is particularly the case for extrusive igneous rocks, which typically have larger dispersion than sedimentary rocks. In this case, geomagnetic SV is large enough that within 20° of the equator both positive and negative inclinations would be expected for basalt flows formed during an interval of constant polarity. Basically, the sign of the inclination cannot be used as a definitive estimate of geomagnetic polarity.

The situation is less problematic for the sedimentary units because the dispersion is generally lower, and therefore, the sign of the inclination is more likely to reflect the polarity. Indeed, we were able to establish an accurate magnetostratigraphy for the interval from 217

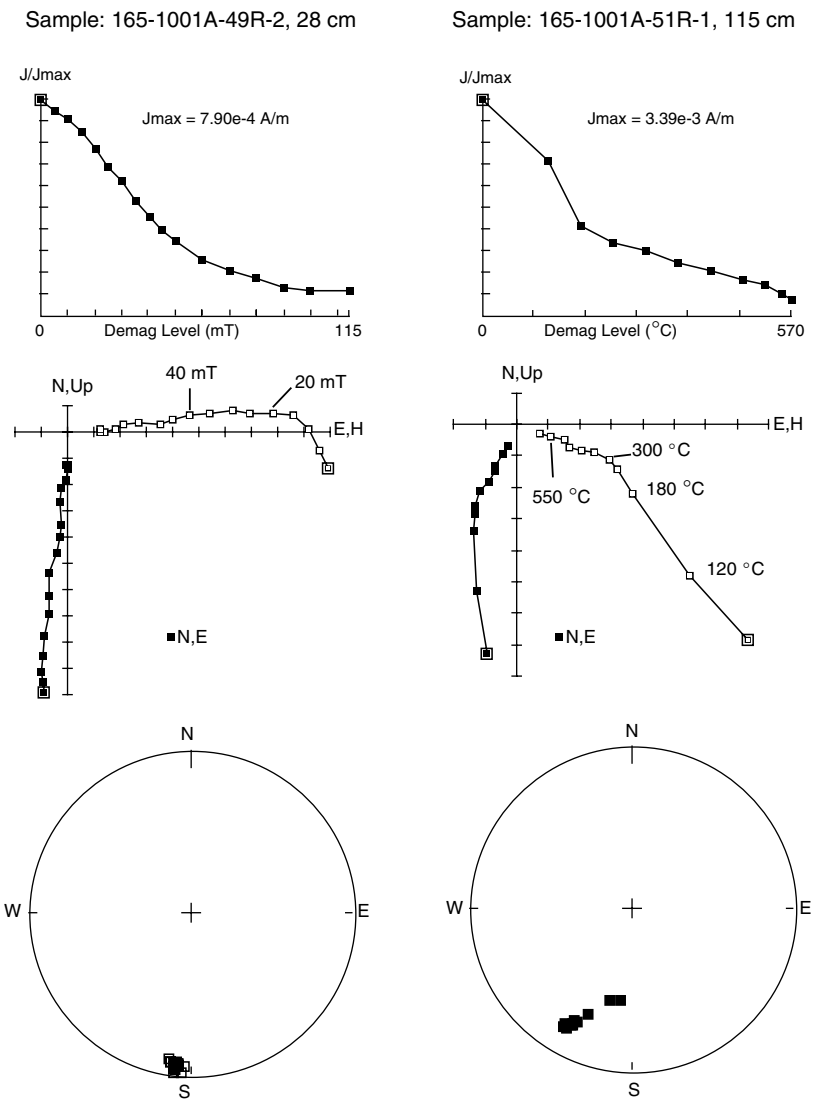

Figure 4. AF and thermal demagnetization results characteristic of some of the better sedimentary rock samples from Site 1001 (Samples 165-1001A-49R-2, 28 cm, and 51R-1, 115 cm). AF demagnetization results show that the magnetic mineral carrying the ChRM has a medium-to-high coercivity whereas the drill-string overprint has a low coercivity. This allows the drill-string overprint to be removed by ~15–20 mT. Thermal demagnetization results show that the steep drill-string overprint is removed by ~300°C with the shallow ChRM direction remaining. See Figure 2 caption for diagram descriptions.

to 396 mbsf at Site 1001, which spans Chron 27R to 31R (pp. 314–315 of Sigurdsson, Leckie, Acton, et al., 1997; V. Louvel and B. Galbrun, unpubl. data; King et al., Chap. 8, this volume). Even within these well-defined chronozones, the sign of the inclination is not always indicative of polarity. For example, the interval from 351 to 355 mbsf at Site 1001 is unambiguously part of Chronozone 29R. Within this interval, however, the inclination estimated from discrete samples is not always negative, but instead varies from – 9.6° to 1.1°. Unfortunately, we could not establish the magnetic polarity for the sedimentary units other than for the interval from 217 to 396 mbsf at Site 1001.

If the polarity is unknown and both polarities are present in a set of paleolatitude data, the average paleolatitude will be less than the true paleolatitude (Fig. 7). Alternatively, if inclinations with negative values are assumed to have the opposite polarity as those with positive values, inverting the negative values (taking their absolute value) will produce a new set of paleolatitudes whose mean will be greater than the true paleolatitude. In either case, the bias can be as large or even larger than the AD bias noted in past studies.

We correct for the POAM bias using a method developed by G.D. Acton (unpubl. data). The correction is based on Monte Carlo simulations that use global SV models to predict the difference between true paleolatitudes and expected (observed) paleolatitudes. Here, we use Harrison's (1980) estimates of the precision parameter (κ) as a function of latitude for the basalts, which gives values of $\kappa \approx 40$ for near-equatorial sites (Fig. 8). We would expect that κ would be larger than this for the sedimentary units because each sedimentary sample partially averages SV. Indeed, using the method of McFadden and Reid (1982), we find that κ varies from 70 to 110 for subsets of data from the interval 217–396 mbsf at Site 1001 where the polarity is known. We therefore use $\kappa = 80$ as a representative value for the sedimentary intervals where the polarity is unknown.

The method works as follows:

1. Generate a set of N (typically 10,000 in this study) Fisherian distributed virtual geomagnetic poles (VGPs) about a known pole location (the north pole) and with a known dispersion.
2. Compute the inclinations that would be observed at a site with known latitude from each of the N VGPs. Repeat this at sites going from 0° to 90° latitude at increments of 0.1°.
3. Take the absolute values of the inclinations and convert these to a set of paleolatitudes.
4. Compute the mean paleolatitude at each synthetic site. This is the expected paleolatitude (i.e., what one would expect to ob-

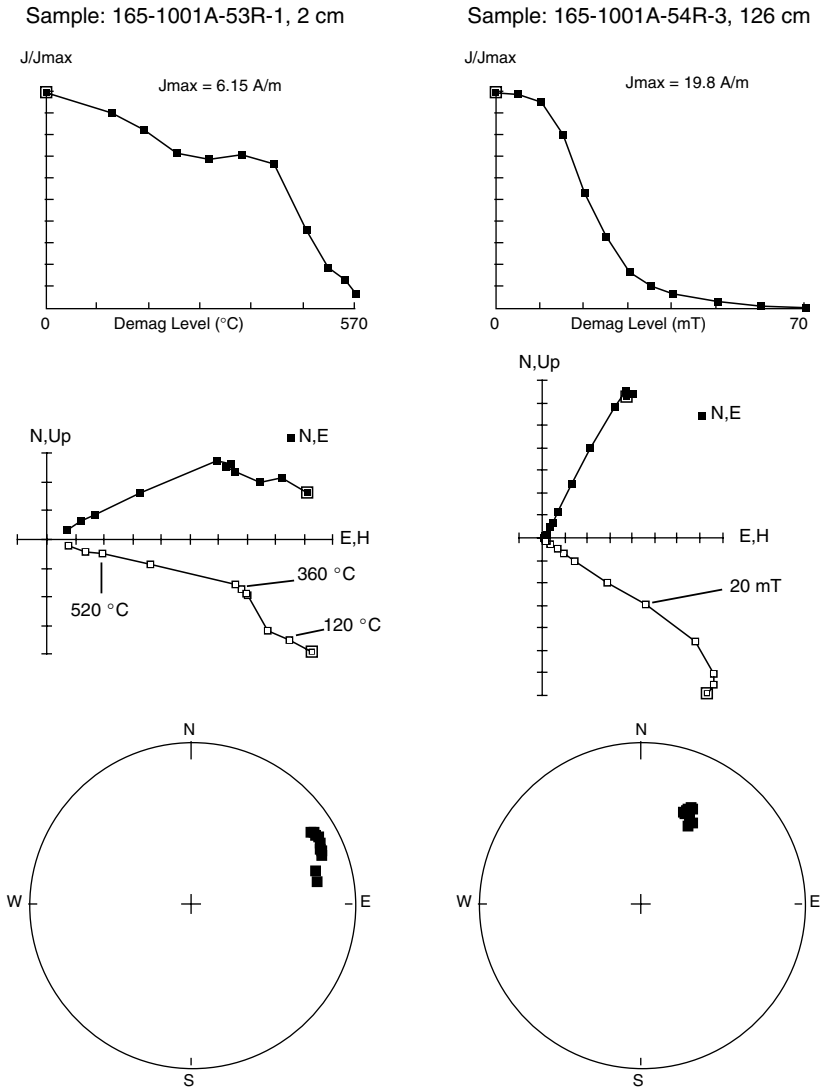

Figure 5. AF and thermal demagnetization results characteristic of some of the better basalt samples from Site 1001. Thermal demagnetization results for Sample 165-1001A-53R-1, 2 cm (left three plots), show that the magnetic mineral carrying the ChRM has an unblocking temperature concentrated between 420°C and 570°C. The steep drill-string overprint is removed by ~360°C with the shallow ChRM direction remaining. AF demagnetization results for Sample 165-1001A-54R-3, 126 cm, shows that the magnetic mineral carrying the ChRM has a medium coercivity whereas the drill-string overprint has a low coercivity. This allows the drill-string overprint to be removed by about 15–20 mT. See Figure 2 caption for diagram descriptions.

serve from a real data set). An example table is shown for κ = 40 and 80, N = 10,000, and for known paleolatitudes of 0°–90° (Table 19). From this table, it is clear that we expect to get a value that is biased away from the equator (i.e., the expected paleolatitude is larger than the true paleolatitude). The difference between the expected and the true paleolatitudes gives the bias correction, T.

5. Take the absolute values of the observed inclinations, convert these to paleolatitudes, and then compute a mean paleolatitude (λ_{mean}). Compare this value to the expected values determined from the Monte Carlo simulations in Table 19. The true paleolatitude (λ_{true}), corresponds to the unbiased estimate of the paleolatitude ($\lambda_{unbiased}$) for the real data. The relationships are

$$T(\lambda_{exp}) = \lambda_{exp} - \lambda_{true} \approx T(\lambda_{mean}) \text{ and} \quad (1)$$

$$\lambda_{unbiased} = \lambda_{mean} - T \approx \lambda_{true}, \quad (2)$$

where $T(\lambda_{exp})$ refers to the bias correction at an expected paleolatitude of λ_{exp}. For example, if we compute an observed mean paleocolatitude of 8°, the unbiased paleolatitude would be 4.5° assuming κ = 40 and using Table 19. The bias correction, T(8°), is 3.5° in this case. This bias correction includes both the AD and POAM biases, though the former is negligible for Caribbean data.

The uncertainty calculation for the unbiased paleolatitude follows from that given by Cox and Gordon (1984, pp. 56–57). We define S_T as the best estimate of total standard error in the paleolatitude, where

$$S_T^2 = S_R^2 + S_S^2. \quad (3)$$

S_R is the standard error attributed to random errors in the paleolatitudes and S_S is the standard error attributed to systematic errors. These are all univariate standard errors. Just like the mean paleolatitude, the value of S_R can be biased by the polarity ambiguity. It must therefore be estimated either from the dispersion of the paleolatitudes or from the value expected from SV. We define S_{SV} as the standard error expected owing to SV, and S_B as the between-flow standard error for basalts or the between-sample standard error for sediments. For N independent samples of the geomagnetic field, $S_{SV} = 81°/\sqrt{2\kappa N}$. S_B is estimated from the dispersion of the paleolatitudes. We then take S_R to be the larger of S_{SV} or S_B. We assign S_S a value of 2° to account for systematic errors, such as those resulting from deviation of the drill hole from vertical. The upper $S_{(+)}$ and lower $S_{(-)}$ bounds for the standard error of the unbiased paleolatitude are then given by

$$S_{(-)} = \lambda_{mean} - S_T - T(\lambda_{mean} - S_T), \quad (4)$$

with the restriction that $S_{(-)} \geq 0$, and

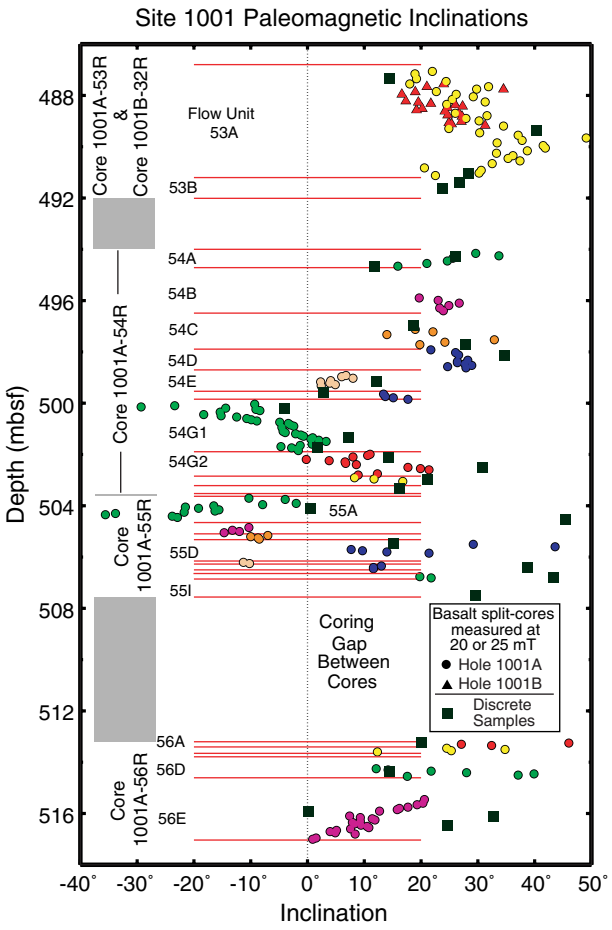

Figure 6. Inclinations from basalt cores from Site 1001. Flow units (53A, 53B, etc.) are labeled to the left (see also Tables 1 and 15), and flow-unit contacts are shown by the horizontal lines. Split-core inclinations from Hole 1001A are shown by circles with different shades used for each flow unit. Split-core inclinations from Hole 1001B are shown by solid triangles. The solid squares indicate inclinations computed from principal-component analysis of demagnetization data for discrete samples from Hole 1001A.

$$S_{(+)} = \lambda_{mean} + S_T - T(\lambda_{mean} + S_T). \quad (5)$$

The error bounds are restricted to positive paleolatitudes because we are analyzing the absolute values of the inclinations. For our example case with λ_{mean} and $\kappa = 40$, lets assume that S_T is 3.3°. Then $S_{(-)}$ = 8.0° – 3.3° – T(8.0° – 3.3°) = 8.0° – 3.3° – 7.2°, but because $S_{(-)}$ must be ≥0, the best estimate of the lower bound is 0.0°. Similarly, $S_{(+)}$ = 8.0° + 3.3° – T(8.0° + 3.3°) = 8.0° + 3.3° – 1.0° = 10.3°. The unbiased mean lies between 0° and 10.3°, which is denoted here as $\lambda_{unbiased}$ = 4.5° (+5.8° or –4.5°; 1σ). The 95% confidence limits are similarly calculated except that S_T is replaced by 1.96 S_T in equations 4 and 5.

RESULTS

Site 998

A total of 56 samples from Cores 165-998A-1H through 11H (0–5 Ma), 18 samples from Cores 165-998A-31X through 62X (22–34 Ma), and 18 samples from Cores 165-998B-3R through 23R (32–44 Ma) were stepwise AF demagnetized. Only 24 of these samples gave linear demagnetization paths and ChRM inclinations, with the rest either giving scattered directions with no ChRM or steep directions indicative of the drill-string overprint (Tables 11, 16; Fig. 2).

These data were combined into two groups, one spanning 0–100 mbsf (2.1 Ma) and the other spanning 582–740 mbsf (38 Ma), with no data from the intervening intervals (Table 20; Fig. 9). In addition, the results from stepwise thermal demagnetization of 33 samples from Cores 165-998B-32R through 37R (848–902 mbsf; 49–52 Ma) were provided by V. Louvel and B. Galbrun (unpubl. data) (Table 16). The mean paleolatitude when corrected for the POAM bias is 7.9° (with asymmetrical 95% confidence limits of +5.1° or –7.9°) for the 33 samples. Site 998 would therefore have moved at least 6.5° northward over the past 50 m.y. or at an average rate of at least 14 km/m.y.

Site 998 only provides a proxy for the northward motion of the Caribbean plate because it has not been a part of that plate since the Eocene, though it has maintained a position to the north of the Caribbean plate (e.g., Pindell et al., 1988). The amount of northward motion estimated from this sparse data set is greater than that found in the larger data sets from Sites 999 and 1001, but is consistent within the relatively large uncertainties.

Site 999

A total of 152 samples from Hole 999A and 146 samples from Hole 999B were stepwise AF and thermal demagnetized (Table 12). In general, AF demagnetization was more successful at removing the drill-string overprint than was thermal demagnetization. Typically, AF demagnetization between 25 and 70 mT was best at resolving the ChRM, whereas thermal demagnetization above 500°C was needed to remove the drill-string overprint. Of the 298 samples, 113 gave ChRMs that pass the discrete sample rejection criteria (Table 17). These span from 2 to 1065 mbsf, nearly the entire cored interval, though data are absent from 300 to 550 mbsf.

The paleolatitudes from the 113 samples and mean paleolatitudes for 10 intervals (0–50, 50–100, 100–200, 200–300, 500–600, 600–700, 700–800, 800–900, 900–1000, and 1000–1065 mbsf; Table 21) are plotted against depth in Figure 10. Lines fit through these indicate the Caribbean plate has moved northward at ~14 km/m.y. Over the past 65 m.y. this gives a total of 8° of northward translation, which places Site 999 very near the equator at the time of the K/T boundary impact event.

Site 1000

Split-core results obtained during Leg 165 had indicated that the intensity of magnetization was extremely low below 22.5 mbsf at Site 1000. The abrupt decrease in magnetization was attributed to reduction diagenesis. In addition, coring only reached limestones of early Miocene age. Therefore, the amount of latitudinal motion recorded by these sedimentary units would likely be small at best.

Nonetheless, we progressively AF demagnetized an additional 40 discrete samples to assess further the magnetization (Table 13). None of the samples from depths >22.5 mbsf gave stable ChRM directions and all displayed weak natural remanent magnetizations (NRM), typically $<8 \times 10^{-4}$ A/m. Data from this site do not provide any paleolatitude constraints and are not considered further.

Site 1001

Basalt Cores

As discussed above, progressive demagnetization of discrete paleomagnetic samples from basalt cores indicates that the drill-string overprint is removed by ~15–20 mT (Fig. 5). Because of this and because the split-core data outnumber the discrete by about an order of magnitude, our primary data for the basalt cores are the split-core inclinations after 25 mT demagnetization (or 20 mT when the 25 mT step is not available). We have carefully edited the data to avoid ends of core sections or gaps that occur within the core (see core photos on pp. 740–763 of Sigurdsson, Leckie, Acton, et al. [1997]). This process left us with 230 inclination estimates. This data set (Table 15)

Table 19. Expected (observed) paleolatitudes and their relationship to the true paleolatitude.

	Precision parameter = 40		Precision parameter = 80	
True paleolatitude	Expected paleolatitude	Bias correction	Expected paleolatitude	Bias correction
0.00	7.17	7.17	5.07	5.07
0.10	7.17	7.07	5.07	4.97
0.20	7.17	6.97	5.07	4.87
0.30	7.17	6.87	5.08	4.78
0.40	7.17	6.77	5.08	4.68
0.50	7.17	6.67	5.08	4.58
0.60	7.18	6.58	5.09	4.49
0.70	7.18	6.48	5.09	4.39
0.80	7.19	6.39	5.10	4.30
0.90	7.19	6.29	5.11	4.21
1.00	7.20	6.20	5.12	4.12
1.10	7.21	6.11	5.13	4.03
1.20	7.22	6.02	5.14	3.94
1.30	7.22	5.92	5.16	3.86
1.40	7.23	5.83	5.17	3.77
1.50	7.25	5.75	5.19	3.69
1.60	7.26	5.66	5.21	3.61
1.70	7.27	5.57	5.23	3.53
1.80	7.28	5.48	5.25	3.45
1.90	7.30	5.40	5.27	3.37
2.00	7.31	5.31	5.29	3.29
2.10	7.33	5.23	5.32	3.22
2.20	7.35	5.15	5.34	3.14
2.30	7.37	5.07	5.37	3.07
2.40	7.39	4.99	5.40	3.00
2.50	7.41	4.91	5.43	2.93
2.60	7.43	4.83	5.46	2.86
2.70	7.45	4.75	5.49	2.79
2.80	7.47	4.67	5.52	2.72
2.90	7.50	4.60	5.56	2.66
3.00	7.52	4.52	5.59	2.59
3.10	7.55	4.45	5.63	2.53
3.20	7.57	4.37	5.67	2.47
3.30	7.60	4.30	5.71	2.41
3.40	7.63	4.23	5.75	2.35
3.50	7.66	4.16	5.79	2.29
3.60	7.69	4.09	5.83	2.23
3.70	7.72	4.02	5.87	2.17
3.80	7.75	3.95	5.92	2.12
3.90	7.78	3.88	5.96	2.06
4.00	7.81	3.81	6.01	2.01
4.10	7.85	3.75	6.05	1.95
4.20	7.88	3.68	6.10	1.90
4.30	7.92	3.62	6.15	1.85
4.40	7.95	3.55	6.20	1.80
4.50	7.99	3.49	6.25	1.75
4.60	8.03	3.43	6.31	1.71
4.70	8.07	3.37	6.36	1.66
4.80	8.11	3.31	6.41	1.61
4.90	8.15	3.25	6.47	1.57
5.00	8.19	3.19	6.52	1.52
5.10	8.23	3.13	6.58	1.48
5.20	8.27	3.07	6.64	1.44
5.30	8.31	3.01	6.70	1.40
5.40	8.36	2.96	6.76	1.36
5.50	8.40	2.90	6.82	1.32
5.60	8.45	2.85	6.88	1.28
5.70	8.50	2.80	6.94	1.24
5.80	8.54	2.74	7.00	1.20
5.90	8.59	2.69	7.07	1.17
6.00	8.64	2.64	7.13	1.13
6.10	8.69	2.59	7.20	1.10
6.20	8.74	2.54	7.26	1.06
6.30	8.79	2.49	7.33	1.03
6.40	8.84	2.44	7.40	1.00
6.50	8.89	2.39	7.47	0.97
6.60	8.94	2.34	7.54	0.94
6.70	9.00	2.30	7.61	0.91
6.80	9.05	2.25	7.68	0.88
6.90	9.10	2.20	7.75	0.85
7.00	9.16	2.16	7.82	0.82
7.10	9.21	2.11	7.89	0.79
7.20	9.27	2.07	7.97	0.77
7.30	9.33	2.03	8.04	0.74
7.40	9.39	1.99	8.12	0.72
7.50	9.44	1.94	8.19	0.69
7.60	9.50	1.90	8.27	0.67
7.70	9.56	1.86	8.34	0.64
7.80	9.62	1.82	8.42	0.62
7.90	9.68	1.78	8.50	0.60
8.00	9.74	1.74	8.58	0.58
8.10	9.81	1.71	8.65	0.55
8.20	9.87	1.67	8.73	0.53
8.30	9.93	1.63	8.81	0.51
8.40	9.99	1.59	8.89	0.49
8.50	10.06	1.56	8.97	0.47
8.60	10.12	1.52	9.05	0.45
8.70	10.19	1.49	9.14	0.44
8.80	10.25	1.45	9.22	0.42
8.90	10.32	1.42	9.30	0.40
9.00	10.39	1.39	9.38	0.38
9.10	10.46	1.36	9.47	0.37
9.20	10.52	1.32	9.55	0.35
9.30	10.59	1.29	9.64	0.34
9.40	10.66	1.26	9.72	0.32
9.50	10.73	1.23	9.81	0.31
9.60	10.80	1.20	9.89	0.29
9.70	10.87	1.17	9.98	0.28
9.80	10.94	1.14	10.07	0.27
9.90	11.01	1.11	10.15	0.25
10.00	11.09	1.09	10.24	0.24
10.10	11.16	1.06	10.33	0.23
10.20	11.23	1.03	10.42	0.22
10.30	11.30	1.00	10.50	0.20
10.40	11.38	0.98	10.59	0.19
10.50	11.45	0.95	10.68	0.18
10.60	11.53	0.93	10.77	0.17
10.70	11.60	0.90	10.86	0.16
10.80	11.68	0.88	10.95	0.15
10.90	11.75	0.85	11.04	0.14
11.00	11.83	0.83	11.13	0.13
11.10	11.90	0.80	11.22	0.12
11.20	11.98	0.78	11.31	0.11
11.30	12.06	0.76	11.40	0.10
11.40	12.14	0.74	11.49	0.09
11.50	12.21	0.71	11.59	0.09
11.60	12.29	0.69	11.68	0.08
11.70	12.37	0.67	11.77	0.07
11.80	12.45	0.65	11.86	0.06
11.90	12.53	0.63	11.96	0.06
12.00	12.61	0.61	12.05	0.05
12.10	12.69	0.59	12.14	0.04
12.20	12.77	0.57	12.24	0.04
12.30	12.85	0.55	12.33	0.03
12.40	12.93	0.53	12.42	0.02
12.50	13.01	0.51	12.52	0.02
12.60	13.10	0.50	12.61	0.01
12.70	13.18	0.48	12.70	0.00
12.80	13.26	0.46	12.80	0.00
12.90	13.34	0.44	12.89	–0.01
13.00	13.43	0.43	12.99	–0.01
13.10	13.51	0.41	13.08	–0.02
13.20	13.59	0.39	13.18	–0.02
13.30	13.68	0.38	13.27	–0.03
13.40	13.76	0.36	13.37	–0.03
13.50	13.85	0.35	13.47	–0.03
13.60	13.93	0.33	13.56	–0.04
13.70	14.02	0.32	13.66	–0.04
13.80	14.11	0.31	13.75	–0.05
13.90	14.19	0.29	13.85	–0.05
14.00	14.28	0.28	13.95	–0.05
14.10	14.36	0.26	14.04	–0.06
14.20	14.45	0.25	14.14	–0.06
14.30	14.54	0.24	14.23	–0.07
14.40	14.62	0.22	14.33	–0.07
14.50	14.71	0.21	14.43	–0.07
14.60	14.80	0.20	14.52	–0.08
14.70	14.89	0.19	14.62	–0.08
14.80	14.97	0.17	14.72	–0.08
14.90	15.06	0.16	14.82	–0.08
15.00	15.15	0.15	14.91	–0.09
16.00	16.05	0.05	15.89	–0.11
17.00	16.96	–0.04	16.88	–0.12
18.00	17.89	–0.11	17.86	–0.14
19.00	18.83	–0.17	18.85	–0.15
20.00	19.78	–0.22	19.84	–0.16
21.00	20.74	–0.26	20.83	–0.17
22.00	21.71	–0.29	21.83	–0.17
23.00	22.68	–0.32	22.82	–0.18
24.00	23.65	–0.35	23.81	–0.19
25.00	24.63	–0.37	24.80	–0.20
26.00	25.61	–0.39	25.79	–0.21
27.00	26.59	–0.41	26.79	–0.21
28.00	27.57	–0.43	27.78	–0.22
29.00	28.55	–0.45	28.77	–0.23
30.00	29.53	–0.47	29.76	–0.24
31.00	30.52	–0.48	30.75	–0.25
32.00	31.50	–0.50	31.74	–0.26
33.00	32.48	–0.52	32.73	–0.27
34.00	33.46	–0.54	33.72	–0.28
35.00	34.44	–0.56	34.72	–0.28
36.00	35.42	–0.58	35.71	–0.29
37.00	36.40	–0.60	36.70	–0.30
38.00	37.38	–0.62	37.69	–0.31

Table 19 (continued).

	Precision parameter = 40		Precision parameter = 80	
True paleolatitude	Expected paleolatitude	Bias correction	Expected paleolatitude	Bias correction
39.00	38.36	–0.64	38.67	–0.33
40.00	39.34	–0.66	39.66	–0.34
41.00	40.31	–0.69	40.65	–0.35
42.00	41.29	–0.71	41.64	–0.36
43.00	42.26	–0.74	42.63	–0.37
44.00	43.24	–0.76	43.62	–0.38
45.00	44.21	–0.79	44.60	–0.40
46.00	45.19	–0.81	45.59	–0.41
47.00	46.16	–0.84	46.58	–0.42
48.00	47.13	–0.87	47.56	–0.44
49.00	48.10	–0.90	48.55	–0.45
50.00	49.07	–0.93	49.53	–0.47
51.00	50.03	–0.97	50.52	–0.48
52.00	51.00	–1.00	51.50	–0.50
53.00	51.96	–1.04	52.48	–0.52
54.00	52.92	–1.08	53.46	–0.54
55.00	53.88	–1.12	54.44	–0.56
56.00	54.84	–1.16	55.42	–0.58
57.00	55.79	–1.21	56.40	–0.60
58.00	56.75	–1.25	57.38	–0.62
59.00	57.70	–1.30	58.35	–0.65
60.00	58.64	–1.36	59.33	–0.67
61.00	59.58	–1.42	60.30	–0.70
62.00	60.52	–1.48	61.27	–0.73
63.00	61.45	–1.55	62.24	–0.76
64.00	62.38	–1.62	63.21	–0.79
65.00	63.30	–1.70	64.17	–0.83
66.00	64.21	–1.79	65.13	–0.87
67.00	65.12	–1.88	66.09	–0.91
68.00	66.01	–1.99	67.04	–0.96
69.00	66.90	–2.10	67.99	–1.01
70.00	67.77	–2.23	68.93	–1.07
71.00	68.63	–2.37	69.87	–1.13
72.00	69.47	–2.53	70.79	–1.21
73.00	70.30	–2.70	71.71	–1.29
74.00	71.10	–2.90	72.62	–1.38
75.00	71.88	–3.12	73.51	–1.49
76.00	72.64	–3.36	74.39	–1.61
77.00	73.36	–3.64	75.24	–1.76
78.00	74.06	–3.94	76.07	–1.93
79.00	74.71	–4.29	76.87	–2.13
80.00	75.33	–4.67	77.64	–2.36
81.00	75.91	–5.09	78.37	–2.63
82.00	76.43	–5.57	79.05	–2.95
83.00	76.91	–6.09	79.67	–3.33
84.00	77.34	–6.66	80.24	–3.76
85.00	77.70	–7.30	80.73	–4.27
86.00	78.01	–7.99	81.15	–4.85
87.00	78.25	–8.75	81.48	–5.52
88.00	78.43	–9.57	81.73	–6.27
89.00	78.54	–10.46	81.88	–7.12
90.00	78.58	–11.42	81.94	–8.06

Notes: Expected paleolatitudes are computed from Monte Carlo simulations, in which 10,000 synthetic paleomagnetic poles are generated about the north pole. Results are given for when the precision parameter is set to 40 and 80. The bias correction includes biases caused by the polarity ambiguity bias and by the angular distance bias (see text).

agrees well with mean inclinations determined from PCA of progressively demagnetized discrete samples (Fig. 6; Table 18). Only in the interval from 504.5 to 508 mbsf is there significant disagreement between split-core and discrete results, with both data sets displaying large variations in inclination over this short interval.

The data are divided into groups based on which "flow unit" they occur within, using the flow-unit divisions in Table 1 (Fig. 6). In some cases, two or more flow units may belong to the same flow or may belong to two or more flows that were extruded within a short interval of time (less than a few hundred years) relative to geomagnetic SV. In these cases, the variation in inclination from unit to unit can be used to group the flow units into units that represent independent samples of the geomagnetic field, which we refer to as "SV units." The goal of this procedure is to determine how many independent samples of the geomagnetic field are present within the 32-m-long cored interval in order to assess how well geomagnetic SV has been averaged. The more SV units present, the more time likely sampled by the volcanic rocks and the greater the likelihood that the mean paleomagnetic inclination represents that of a time-averaged, geocentric axial dipole field.

Flow-unit mean inclinations from stratigraphically adjacent units were compared. If a mean inclination was within three standard errors of the mean inclination of stratigraphically adjacent units (i.e., the inclinations differ insignificantly at greater than the 99% confidence level), then the inclinations for the units were combined and a SV-unit mean inclination was computed. Similarly, we converted each inclination into a paleolatitude and computed a SV-unit mean paleolatitude. Overall, the grouping process resulted in 27 flow units giving 12 SV units. Note that the units have both positive and negative inclinations, which could indicate field reversals or could simply reflect geomagnetic SV during an interval of constant polarity.

The 12 SV-unit mean paleolatitudes, which are used in subsequent calculations of the overall mean paleolatitude, are shown in Figure 11. To calculate the overall mean paleolatitude, we use two different approaches. First, using the age of the overlying limestone and radiometric ages from the basalt (76–80 Ma and 81 ±1 Ma, respectively), we might suspect that the basalts were all deposited in an interval of constant polarity prior to the deposition of the overlying sediment. This would most likely place the basalts entirely within the older portion of Chron 33n (73.619–79.075 Ma) or entirely within Chron 33r (79.075–83.00 Ma). Assuming all the basalts were extruded within an interval of constant polarity gives a mean paleolatitude of 4.3°(N or S) ±6.3°. Alternatively, both polarities could be present, with the basalts possibly being extruded over the interval from Chron 34n to 33n. Making no assumption about the polarity gives an unbiased mean paleolatitude of ±4.5°(+9.7°/–4.5°).

These estimates do not require that the Caribbean plate reside in the Northern Hemisphere, though the polarity through the K/T boundary section at this site clearly indicates a Northern Hemisphere position. Hence, the bulk of the Caribbean plate has likely been in the northern hemisphere since at least 80 Ma. Both basalt estimates place the Caribbean plate ~10° south of its current position. Within the uncertainties, Site 1001 could have been on or very near the equator in the Late Cretaceous.

Discrete Data

A total of 76 samples (30 from basalt cores) from Hole 1001A and 13 samples from Hole 1001B were stepwise AF and thermally demagnetized. Both demagnetization methods typically revealed shallow inclinations after removal of a steep downward overprint direction (Fig. 4). Of the 59 samples from sedimentary units, 28 gave ChRM inclinations. The overprint was difficult to remove in the younger sediments (down to the base of Core 165-1001A-17R at 160 mbsf, middle Miocene age), with no ChRM inclination obtained for cores above this.

In addition, the results from stepwise demagnetization of 138 samples from sedimentary units from Hole 1001A and 141 samples from Hole 1001B were provided by V. Louvel and B. Galbrun (unpubl. data). The combined data set of 308 sample paleolatitudes is subdivided by depth into four intervals down to basaltic basement (160–211, 217–331, 331–396, and 396–484 mbsf).

The magnetostratigraphy (Fig. 12) is well resolved for the interval from 217 to 331 mbsf, corresponding to Chrons 24r–27n, and for the interval from 331 to 396 mbsf, corresponding to Chrons 27r–31r (pp. 314–315 of Sigurdsson, Leckie, Acton, et al., 1997; V. Louvel and B. Galbrun, unpubl. data; King et al., Chap. 8, this volume). Because the polarity of the samples can be ascertained, computation of paleolatitudes is straightforward and gives estimates with smaller uncertainty. To ensure that the mean paleolatitudes for these two intervals did not include samples with uncertain polarities, we excluded samples collected near polarity transitions or within zones where the polarity was uncertain (Fig. 12). Data from within these two intervals are important for several reasons. First, based on the magnetostratigraphy, par-

Table 20. Mean inclinations and paleolatitudes for the basalt units.

Unit name	N	Inclination (°)	Std. error[1]	Paleolatitude	Std. error[2]
Flow unit 53A	57	27.9	0.9		
Flow unit 53B	8	25.4	1.9		
Flow unit 54A	6	25.1	2.6		
Flow unit 54B	6	23.6	0.9		
Flow unit 54C	6	22.0	2.6		
Flow unit 54D	10	26.5	0.7		
SV unit 1	93	26.7	0.7	14.3	0.4
SV unit 2 = Flow unit 54E	8	4.8	0.7	2.4	0.4
SV unit 3 = Flow unit 54F	4	15.0	1.0	7.6	0.5
SV unit 4 = Flow unit 54G1	34	–6.4	1.3	3.3	0.7
Flow unit 54G2	13	10.4	1.7		
Flow unit 54H	3	12.3	2.5		
SV unit 5	16	10.8	1.4	5.5	0.8
Flow unit 55A	14	–17.9	2.6		
Flow unit 55B	4	–12.6	0.9		
SV unit 6	18	–16.7	2.1	8.7	1.2
SV unit 7 = Flow unit 55C	4	–8.6	0.6	4.3	0.3
SV unit 8 = Flow unit 55D	8	30.5	7.6	18.7	5.6
SV unit 9 = Flow unit 55E	2	–10.8	0.6	5.4	0.3
SV unit 10 = Flow unit 55F	3	12.1	0.5	6.1	0.2
Flow unit 55H	2	20.8	1.0		
Flow unit 56A	3	35.2	5.6		
Flow unit 56B	4	24.2	4.6		
Flow unit 56D	7	24.4	4.1		
SV unit 11	16	25.9	2.5	14.0	1.5
SV unit 12 = Flow unit 56E	24	10.5	1.1	5.3	0.6

Notes: Std. error[1] = standard error of the mean inclination; Std. error[2] = standard error of the mean paleolatitude; Paleolatitude = the mean of the absolute value of the sample paleolatitudes. The SV unit mean inclination is the mean calculated from a number (N) of inclination estimates from one or more flow units. Similarly, the SV unit mean paleolatitude is the mean calculated from N paleolatitude estimates from one or more flow units (see text for details).

Table 21. Mean paleolatitudes.

Age (Ma)	Depth range (mbsf)	Mean depth (mbsf)	N	A-mean paleolatitude	S_B	B-mean paleolatitude	Unbiased mean paleolatitude	S_{SV}	S_R	S_T	Std. error of unbiased mean	95% conf. limits for mean paleolatitude
Site 998 (19.49°N, 277.06°E)												
2.1	0-100	40.1	14	19.0	2.2	16.1	19.2	1.7	2.2	3.0	±3.0	+5.9/–6.0
38.0	582-734	655.1	10	14.0	2.2	11.6	14.1	2.0	2.2	3.0	+3.0/–3.2	+5.9/–6.6
50.0	848-903	877.1	33	8.5	1.0	8.6	7.9	1.1	1.1	2.3	+2.7/–3.5	+5.1/–7.9
Site 999 (12.74°N, 281.26°E)												
0.71	0-50	26.8	12	13.0	1.7	13.0	13.0	1.8	1.8	2.7	+2.8/–2.9	+5.4/–6.1
2.1	50-100	70.1	18	12.3	2.0	10.2	12.3	1.5	2.0	2.8	+2.9/–3.2	+5.7/–6.9
3.8	100-200	125.2	11	13.0	2.8	10.8	13.0	1.9	2.8	3.4	+3.6/–3.8	+6.9/–8.5
8.9	200-300	245.4	3	19.4	7.4	23.0	19.6	3.7	7.4	7.7	+7.7/–7.9	+14.8/–19.6
22.7	579-600	581.2	6	10.2	1.3	9.7	10.0	2.6	2.6	3.3	+3.6/–4.3	+6.8/–10.0
27.0	600-700	637.6	13	7.1	1.4	5.7	6.0	1.8	1.8	2.7	+3.5/–6.0	+6.4/–6.0
36.0	700-800	755.7	14	8.0	1.8	7.5	7.2	1.7	1.8	2.7	+3.3/–5.1	+6.1/7.2
44.0	800-900	842.4	18	6.2	0.9	6.1	4.4	1.5	1.5	2.5	+3.8/–4.4	+6.6/–4.4
50.0	900-1000	924.1	8	6.3	1.3	6.3	4.6	2.3	2.3	3.0	+4.4/–4.6	+7.6/–4.6
66.0	1000-1066	1052.8	10	6.2	1.1	4.6	4.4	2.0	2.0	2.8	+4.2/–4.4	+7.3/–4.4
Site 1001 (15.76°N, 285.09°E)												
54.0	160-211	183.0	10	7.5	2.8	8.6	6.5	2.0	2.8	3.4	+4.3/–6.5	+7.8/–6.5
57.0 (Chron 24R-27N)	217-331	284.2	94	5.0	0.3	5.6	5.0	—	0.3	2.0	±2.0	±3.9
65.0 (Chron 27R-31R)	331-396	361.7	68	4.7	0.4	4.4	4.7	—	0.4	2.0	±2.0	±3.9
74.0	396-484	440.3	96	7.5	0.6	5.6	6.5	0.7	0.7	2.1	+2.7/–4.2	+5.0/–6.5
81.0 (basalt)[1]	487-517	502.0	230 (12*)	8.0	1.5		4.5	2.6	2.6	3.3	+5.8/–4.5	+9.7/–4.5
81.0 (basalt)[2]	487-517	502.0	230 (12*)	4.3	2.5		4.3	2.6	2.6	3.3	±3.3	±6.5

Notes: N = number of samples; A-Mean paleolatitude = the mean computed from all N paleolatitude (sample or unit) estimates; B-Mean paleolatitude = the mean computed from two values: (1) the mean paleolatitude of data with positive inclinations, and (2) the mean paleolatitude obtained from the absolute values of data with negative inclinations; S_B = the standard error for the A-mean paleolatitude (the between-sample or between-basalt-unit standard error). The 95% confidence limits for the A-mean and B-mean paleolatitudes can be obtained by multiplying S_R by 1.96. S_{SV} = the expected univariate standard error for N samples assuming the dispersion caused by secular variation is described with a precision parameter of 40; S_R = the standard error attributed to random errors, which is taken to be the larger of the S_B or S_{SV}; S_S = the standard error attributed to systematic errors. We assume this to be 2°, to account for systematic deviations of the borehole from vertical; S_T = the total standard error used for the unbiased mean, which is = $\sqrt{(S_R^2 + S_S^2)}$. * = there were 230 inclination estimates from the split-core basalt samples. These were grouped into 12 independent secular variation units. 81 Ma (basalt)[1]: no assumption is made about polarity of the SV units; 81 Ma (basalt)[2]: polarity assumed to be constant during the extrusion of 12 SV units.

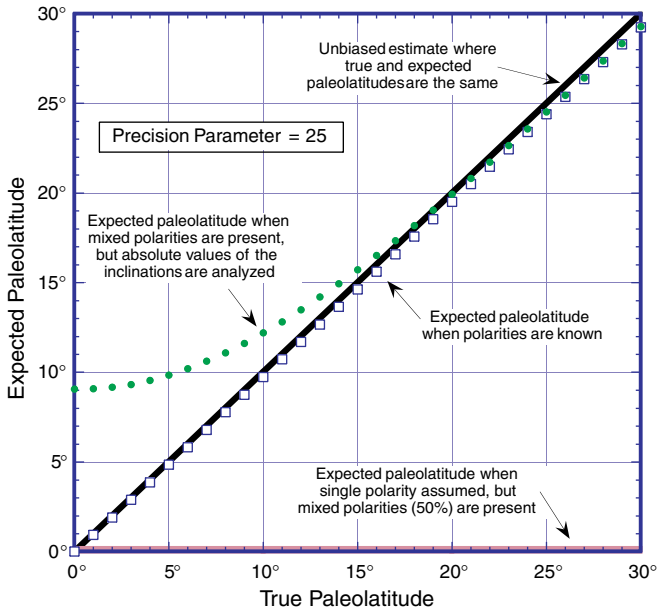

Figure 7. Paleolatitude biases occur when inclination data are analyzed in different ways to get a mean paleolatitude. The diagonal line (thick solid line running from lower left to upper right) represents the desired case, where mean paleolatitude = true paleolatitude. If the geomagnetic polarity of all units sampled is known, the mean paleolatitude is virtually identical to the true paleolatitude for low paleolatitudes (squares). A very large error can occur, however, when the geomagnetic polarity is assumed (gray line running along the bottom of the plot), and in this example the assumption is wrong 50% of the time. Simply analyzing the paleolatitudes computed from the absolute values of the inclinations, however, gives an expected mean paleolatitude that does not depend on assumptions about the polarity (dotted line). These too are biased, but the size of the bias can be estimated (expected values) and then corrected. We use such expected values to correct the mean paleolatitudes presented in this paper. All calculations shown are for the case when the precision parameter (κ) is 25.

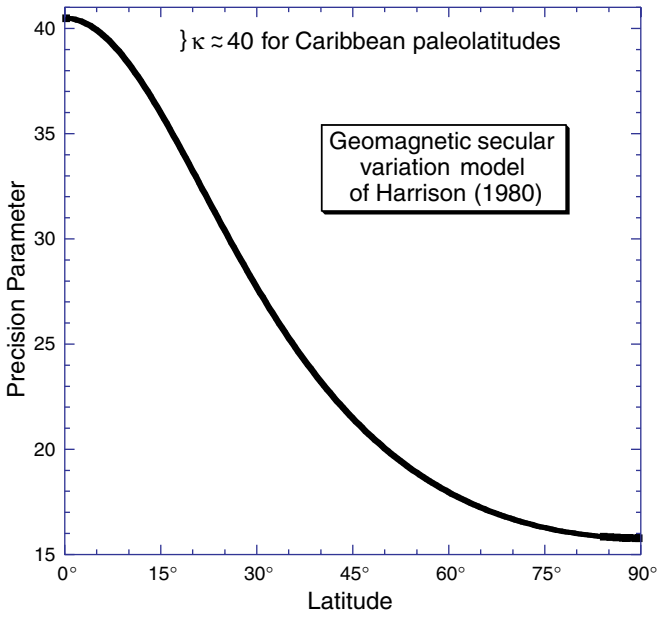

Figure 8. Variation of the precision parameter vs. latitude based on the geomagnetic SV model of Harrison (1980).

ticularly the sign of the inclinations within the chronozones, Site 1001 was in the Northern Hemisphere from Chron 31r to Chron 24r (from 71 to 54 Ma). Second, the smaller 95% confidence limits indicate that Site 1001 was at least 6° south of its current position in the Late Cretaceous and possibly within 1° of the equator.

The mean paleolatitudes for all four intervals indicate that the Caribbean plate has moved progressively northward by ~10° since the Late Cretaceous (Fig. 13). The limestones from 396 to 484 mbsf give a mean inclination of 14.4° and a mean unbiased paleolatitude of 2.9°, which are consistent with the mean inclination of 14.9° and mean unbiased paleolatitude of 4.5° estimated from the 12 SV units from the underlying basalt. The agreement of sedimentary and basalt estimates indicates that biases from inclination shallowing in the sediments are likely small and perhaps negligible.

DISCUSSION

Having considered the paleomagnetic data for each site, it is natural to consider the implications of the combined data set. Sites 999 and 1001 both indicate similar amounts of northward motion for the Caribbean plate over the past 80 m.y. Similarly, Site 998, just to the north of the Caribbean plate, has moved northward at roughly the same rate.

The data from Sites 999 and 1001 can be combined given that the Euler pole that describes the motion of the Caribbean plate relative to the spin axis is not located near the sites. A nearby Euler pole could produce vastly different amounts, and even directions, of latitudinal motion for these sites. Two lines of evidence support a distant Euler pole. First, the similar northward motions estimated at Sites 999 and 1001 are consistent with motions about a distant Euler pole. Second, the long continuous nature of the Swan Island and Oriente transform faults, which separate the North American and Caribbean plates along the Cayman Trough, combined with the motion of the North American plate as recorded by its apparent polar wander path, require that the Caribbean plate has rotated little relative to the spin axis over the past 50 m.y.

Taken together, the results from Sites 999 and 1001 give a clear indication of the change of paleolatitude of the Caribbean plate since the Late Cretaceous. In order to illustrate this point, we plot all the paleolatitudes relative to the current position of Site 999 (Fig. 14). To place the Site 1001 data in this reference frame, we take the change in paleolatitude predicted by each paleolatitude datum (i.e., the current latitude of Site 1001 minus the paleolatitude estimate) and subtract this from the current latitude of Site 999. For example, the 65-Ma paleolatitude estimate from Site 1001 is 4.7°, which translates to a paleolatitude of 1.7° (= 12.74° – [15.76°– 4.7°]) at Site 999. Figure 14 can also be viewed as a plot of northward motion vs. age. Only the 9-Ma mean paleolatitude from Site 999 falls off this plot. Because it was based on only three sample means, far less than the other mean paleolatitudes, and has a large uncertainty, we ignore it in the following discussion, though its inclusion would not change any of the conclusions.

The combined paleolatitudes shown in Figure 14 indicate that Site 999, and hence the southern portion of the Caribbean plate, was near or at the equator in the Late Cretaceous, and has since migrated progressively northward. Data from Sites 999 and 1001 agree well with each other and with a model in which the northward migration occurs at a constant rate. The best-fit rate of the northward motion is 18 ±4 km/m.y., a rate that is consistent with all 13 of the paleolatitude estimates from both sites. Within the uncertainties, however, the data do not preclude changes in the rate of northward motion, such as the example indicated by the thin solid line in Figure 14.

Inclination Biases

Of the 18 mean paleolatitudes estimated in this study, 17 are from sedimentary units. Even though many sediments have been shown to

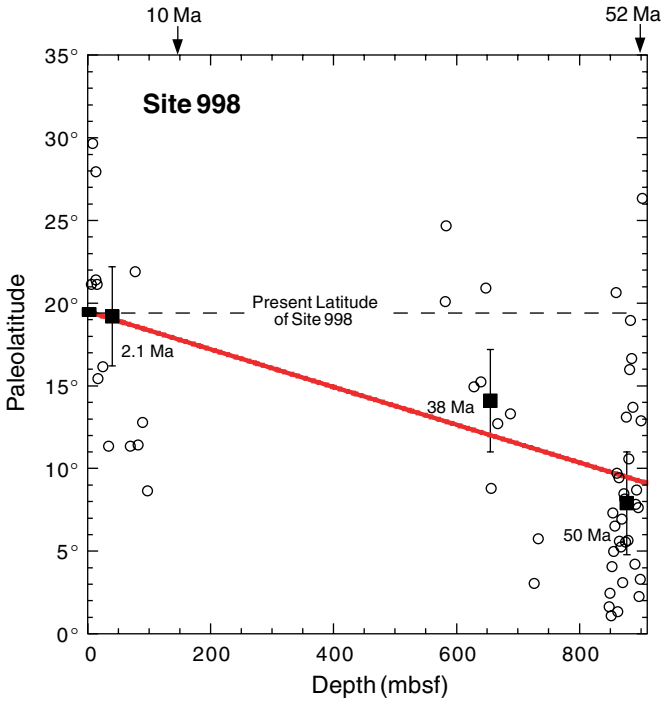

Figure 9. Site 998 paleolatitudes from discrete samples (circles). Also shown are the unbiased mean paleolatitudes (solid squares) and their standard errors (bars). A weighted best-fit line, with a fixed intercept at the present latitude of Site 998, is fit through the mean paleolatitudes. The slope of the line is –0.0114°/m, which corresponds to a rate of northward motion of ~22 km/m.y.

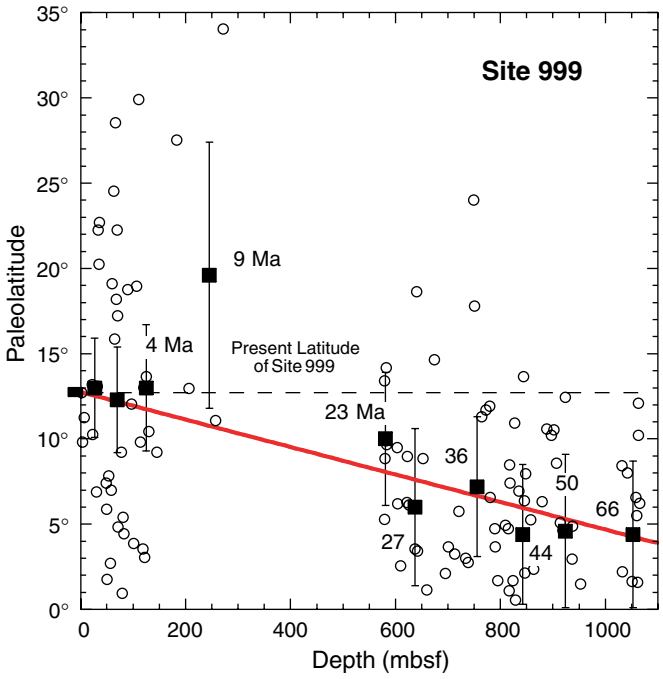

Figure 10. Site 999 paleolatitudes from discrete samples (open circles). Also shown are the unbiased mean paleolatitudes (squares) and their standard errors (bars). The weighted best-fit line, with a fixed intercept at the present latitude of Site 999, is fit through the mean paleolatitudes. The slope of the line is –0.0081°/m, which corresponds to a rate of northward motion of ~14 km/m.y.

be accurate recorders of the geomagnetic field direction (e.g., Opdyke and Henry, 1969; Harrison, 1966; Opdyke, 1972; Kent, 1973), the accuracy of other sedimentary units has been questioned. Several past studies have shown that the inclinations for some sedimentary units are systematically shallower than the known or true inclinations of the paleomagnetic field (e.g., Kent and Spariosu, 1982; Celaya and Clement, 1988; Tarduno, 1990; Gordon, 1990). This systematic shallowing is referred to as the "inclination error." So far, the size of the inclination error has been difficult to resolve as it may depend on a variety of variables, such as the degree of compaction, porosity, water content, sediment composition, degree of bioturbation, and others (e.g., Arason and Levi, 1990a, 1990b; Celaya and Clement, 1988; Tan and Kodama, 1998). What is known, is that the inclination error can be significant, with the error in some cases possibly exceeding 20° (Celaya and Clement, 1988; Tarduno, 1990; Gordon, 1990). These studies and theoretical studies (e.g., Arason and Levi, 1990a, 1990b) have also shown that the error is largest in mid-latitudes and decays at low and high latitudes. The main questions for this study are do the sediments that we use contain an inclination error, and if so, how large is the error?

Though there is no direct evidence that our sedimentary results are biased by the inclination error, there are several observations that suggest that the inclination error is likely small, if present at all. First, as would be expected given the rate of plate motions, the results from young sediments, particularly those younger than 10 Ma, give paleolatitudes consistent with the current latitude. Some of these sediments from Site 999 are from depths >200 mbsf, so a good deal of compaction has taken place. In the study by Celaya and Clement (1988), of the six sites they studied, the inclinations from three sites were biased. At those three sites, the inclination shallowed with depth in the upper 200 m. In our study, the apparent absence of shallowing in the young sediments from the upper 200 m indicates that these Leg 165 sediments record the paleofield direction accurately. Second, the good agreement between the mean paleolatitudes (and mean inclinations) obtained from the basalts and from the overlying sediments, indicates that little if any inclination shallowing has occurred. Within the 95% confidence interval for the basalt estimates, however, large inclination errors could be permitted, but northward motion is required by the data even when pushed to its outer limits. Third, Tan and Kodama (1998) show that the inclination error increases with clay content, with the largest errors occurring in sediments with >40% clay content. For the Nacimiento and Ladd Formations, the two examples used in Tan and Kodama (1998) with <20% clay content, the inclination error was 7°–11°. The clay content for Leg 165 cores is typically <40% (Fig. 15A; pp. 173 and 322 of Sigurdsson, Leckie, Acton, et al., 1997), and is <20% for samples below 400 mbsf from Site 1001 (those samples used in the 74-Ma paleolatitude estimate). Furthermore, the examples used in Tan and Kodama (1998) come from mid-latitude sites, so the size of the inclination error would be larger than expected for low-latitude Caribbean sites. Hence, even if the results of Tan and Kodama were directly applicable to the Caribbean sites, the inclination error would very likely be smaller than ~8°. Fourth, Ceyala and Clement (1988) suggest that the inclination error is present in sediments where the carbonate content is >80%, with clays making up at least part of the remaining composition. They observed no inclination error downcore when the carbonate content was <80%. Though these observations conflict with Tan and Kodama's (1998) findings, it is interesting to note that only the sediments used for the 74-Ma paleolatitude estimate fall within the composition range that Celaya and Clement suggest is biased (Fig. 15A). Finally, consider the paleolatitude estimates from sediments that indicate northward motion, which are all those older than 10 Ma. When the change in paleolatitude from these is plotted against carbonate percentage, water content, or porosity, no obvious trends are apparent (Fig. 15). For example, as water content decreases downhole owing to compaction, Celaya and Clement (1988) suggest

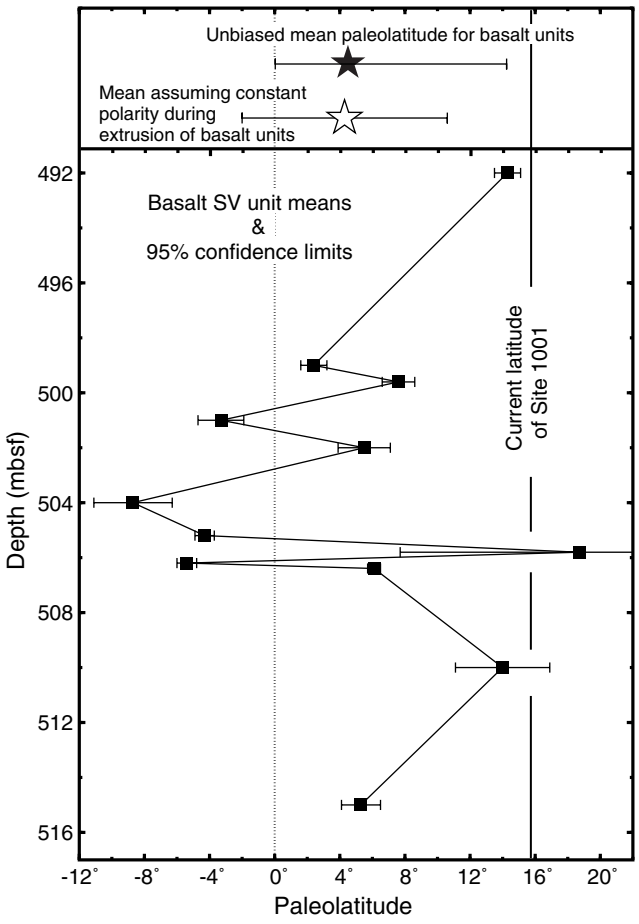

Figure 11. Paleolatitudes for each secular variation (SV) unit (squares) with 95% confidence limits (bars). The mean paleolatitudes and their 95% confidence limits are shown at the top. The solid star is the unbiased mean that makes no assumptions about the polarity of the SV units, whereas the open star is the mean assuming all the SV units were extruded during a period of constant, normal polarity.

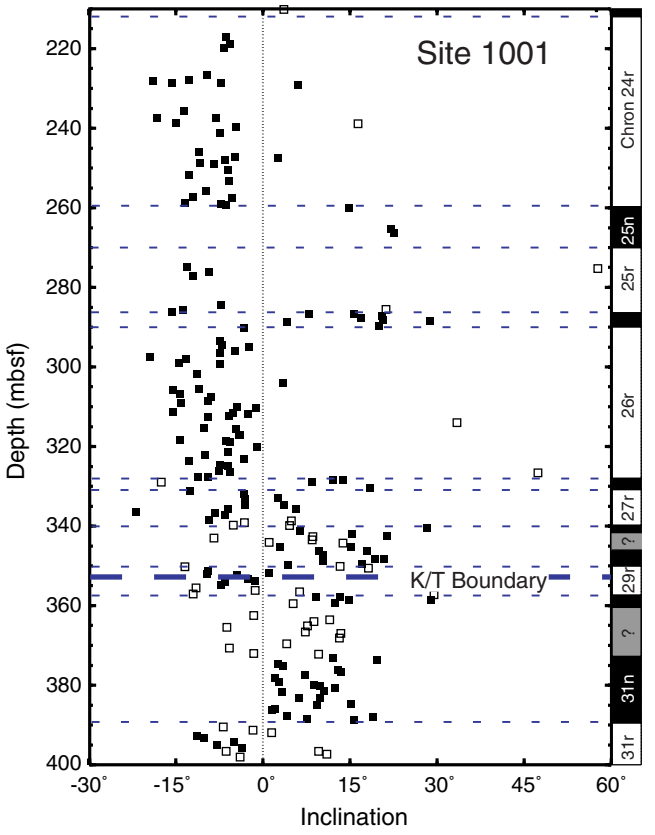

Figure 12. The interval from Site 1001 in which the magnetostratigraphy could be established. The inclinations from PCA of discrete samples are shown by the squares, where open squares are those excluded in the calculations of the mean paleolatitudes in Table 21. These samples are excluded because they are present in transition zones or in zones with poorly resolved polarity, or because their inclinations differ by >20° from other samples in the same chronozone.

that the inclination error should increase. As shown in Figure 15, the water content is actually higher for sediments that indicate the greatest northward translation of the Caribbean plate. This occurs because the overburden at Site 1001 is roughly half that for similar age sediments from Site 999. Even if we consider the data from Site 999 separately from Site 1001, there is poor correlation between compaction-related water loss (or porosity) and northward translation. This is because there is little change in water content or porosity below 600 mbsf at Site 999, though the paleolatitudes continue to decrease with depth.

We conclude that there is little if any supporting evidence that would argue for an inclination error that could explain the observed systematic decrease of paleolatitude with age illustrated in Figure 14. Unfortunately, we cannot prove that an inclination error does not exist. Furthermore, the uncertainties in the paleomagnetic data are large enough to accommodate an inclination error as large as 10° (corresponding to ~5° of paleolatitude) without requiring a complex motion history for the Caribbean plate. Assuming an inclination error of 10° for sediments older than 10 Ma reduces the average rate of northward motion to 8 km/m.y. Larger inclination errors produce a large misfit with the paleolatitude estimated from the basalts and would require that the plate first moved northward and then southward to arrive at its current position. The preferred motion history is, therefore, that shown in Figure 14 in which the Caribbean plate migrates northward at 18 km/m.y. However, the uncertainty interval should likely be expanded to account for the possibility of an inclination error. Assuming that 10° of inclination error represents an upper bound for the 95% confidence interval, then the average rate of northward motion and it 95% confidence region is 18 (+4 or –10) km/m.y.

Motion of the Caribbean Plate Predicted by Tectonic Models

Three fundamentally different types of models have been proposed for the formation and evolution of the Caribbean plate: (1) the "Pacific" model has the Caribbean plate originating in the Mesozoic from a piece of one of the Pacific basin plates, most likely the Farallon plate (e.g., Malfait and Dinkelman, 1972; Pindell and Dewey, 1982; Duncan and Hargraves, 1984; Pindell et al., 1988; Burke, 1988; Pindell, 1994); (2) recent versions of the "intra-American" model have the Caribbean plate originating between North and South America, though well west of its current position (e.g., Klitgord and Schouten, 1986; Meschede and Frisch, 1998); and (3) "Fixist" models indicate the Caribbean plate formed and has maintained roughly its current position (e.g., Morris et al., 1990). This third type of model is incompatible with the paleomagnetic data from this study, as well as being incompatible with the opening history of the Atlantic Ocean (Pindell, 1994), and will not be discussed further.

The most recent versions of the Pacific and intra-American models, as presented by Pindell (Pindell et al., 1988; Pindell and Barrett, 1990; Pindell, 1994) and Meschede and Frisch (1998), respectively,

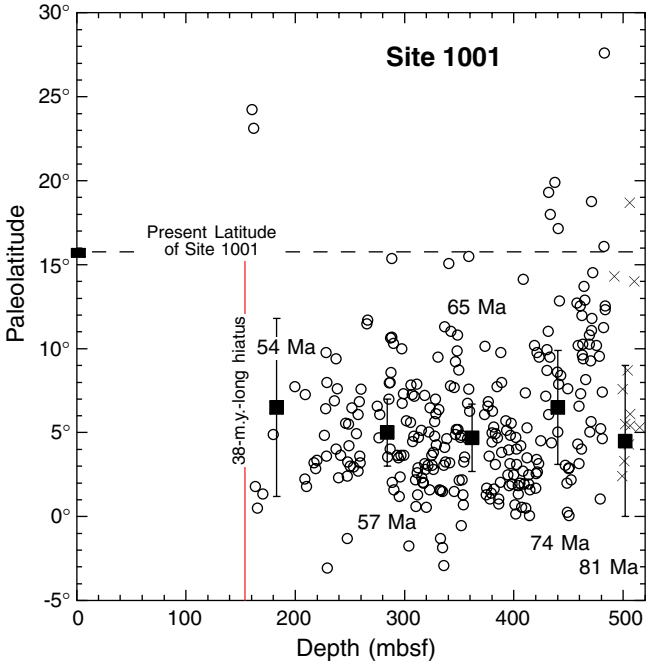

Figure 13. Site 1001 paleolatitudes from discrete sedimentary samples (open circles) and basalt SV units (× symbols). Also shown are the unbiased mean paleolatitudes (solid squares) and their standard errors (bars).

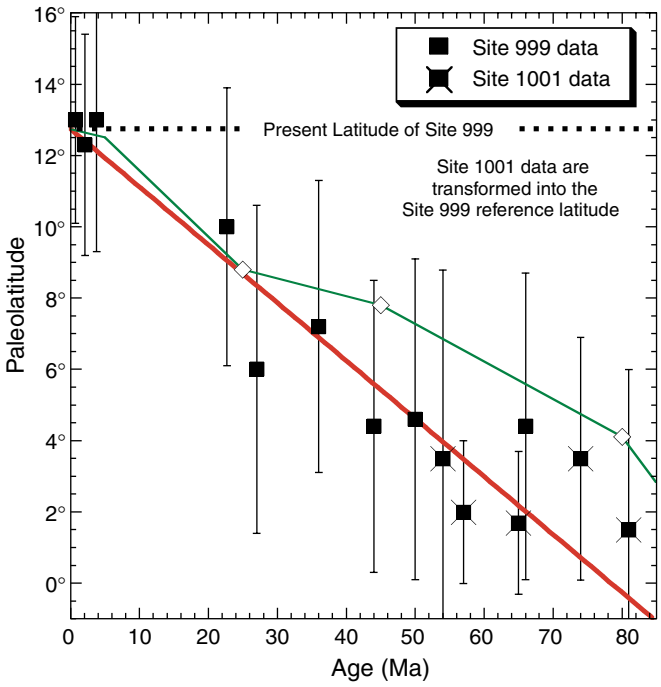

Figure 14. Mean paleolatitudes from Sites 999 and 1001. The best-fit line through these (bold solid line) gives a northward motion rate of 18 km/m.y. for the Caribbean plate. Also shown are the "model" paleolatitudes used in the reconstructions in Figure 16 (diamonds connected by the thin line).

predict very similar motion histories for the Caribbean plate since Campanian time. The two models merge in the Cenozoic, and only relatively minor differences occur in plate boundary geometries back to the early Campanian (~82 Ma). At that time, both models have the Caribbean plate separated from the Pacific basin plates by a subduction zone. The motion predicted by these models only differs significantly for early times, where the Pacific model assumes the Caribbean plate was part of the northeastward migrating Farallon plate.

For the time spanned by our data, the recent versions of these two models differ insignificantly in the motion they predict. Thus, our data cannot be used to support one model over the other. Other observations, such as ages and paleolatitudes of terranes bounding the Caribbean, have been used to support one model or the other (Pindell, 1994; Montgomery et al., 1994; Meschede and Frisch, 1998), though definitive evidence may come only from drilling into the oldest crust of the interior of the Caribbean plate.

The new paleomagnetic data, instead, place paleolatitude constraints on these models. As an example, we have placed a paleolatitude and paleolongitude grid over the reconstructions of Pindell et al. (1988) in Figure 16. The paleolatitudes are selected such that they are consistent with the Caribbean paleomagnetic data, as well as with North American paleomagnetic data and with the reconstructions of North America relative to the hot spots as given by Müller et al. (1993). The paleolongitudes are from the hot-spot reconstructions alone. To illustrate that the grid violates none of the Caribbean paleomagnetic data, we show the position of Sites 999 and 1001 in each panel of Figure 16 and then plot the reconstructed paleolatitudes of Site 999 in Figure 14.

The combined paleomagnetic and hot-spot data suggest the rate of northward motion for the Caribbean plate was slower in the Late Cretaceous to the Oligocene than subsequently. This seems reasonable when the motion of the Caribbean plate is considered relative to North America. For example, the 30-Ma paleomagnetic pole for North America (Diehl et al., 1988) can be used to estimate the average rate of northward motion for a point on the North American plate just north of the Caribbean plate. This pole gives a northward motion rate of 21 km/m.y. for North America averaged over the past 30 m.y. The rate of northward motion of the Caribbean plate would be slightly faster than this because the Caribbean plate was moving east-northeast relative to North America during this time. Similarly, paleomagnetic data from North America (Diehl et al., 1983; Gordon, 1984; Acton and Gordon, 1990) indicate that the southern portion of the North American plate moved southward from the Late Cretaceous to the Eocene. The reconstructions of Pindell et al. (1988) illustrate that the Caribbean plate had a larger northward component of motion relative to North America in the Late Cretaceous to Eocene (~80–40 Ma) than in subsequent times. Thus, over this interval, the net motion of the Caribbean plate relative to the spin axis was still northward, but at a rate slower than that since 30 Ma (Figs. 14, 16).

The paleolongitudes illustrate that the North American plate had a large westward component of motion, which averaged ~50 km/m.y. from 80 to 45 Ma. Over this same time interval, the Caribbean plate also moved westward relative to the hot spots, though at a slower rate of ~34 km/m.y. Since 45 Ma, the North American plate has continued moving westward at an average rate of 24 km/m.y, whereas the Caribbean plate has moved negligibly.

Has the Caribbean Lithosphere Passed over the Galapagos Hot Spot?

In one version of the Pacific model, the lithosphere that became the Caribbean plate was thickened as it passed over an incipient Galapagos hot spot in the Late Cretaceous (Duncan and Hargraves, 1984; Burke, 1988). At this time, the Galapagos hot spot would have been in its plume-head stage. Lithosphere above the plume head, which would have been part of the Farallon plate, was thickened (8–20 km thick) and became part of the Caribbean igneous province. Afterward, the Farallon plate and this oceanic plateau migrated northward and eastward away from the equatorial Galapagos hot spot. In this

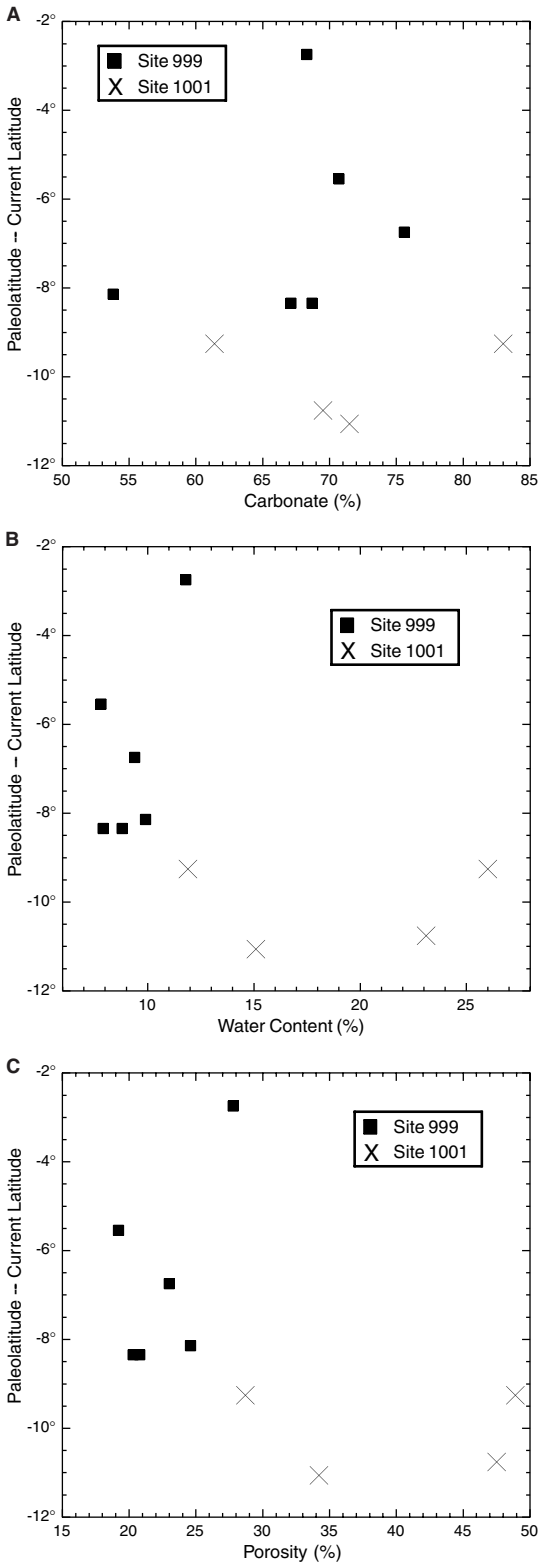

Figure 15. Change in latitude (paleolatitude minus the current latitude) from the paleomagnetic data of Sites 999 and 1001 are plotted vs. percent (**A**) carbonate, (**B**) water content, and (**C**) porosity. Only data from units older than 10 Ma are shown. No clear correlation occurs between the change in latitude and either water content or porosity, which would indicate that any compaction-related inclination error is negligible (see "Discussion" in text).

version of the Pacific model, this overly thickened piece of lithosphere became the core of the Caribbean plate.

The paleomagnetic data (Fig. 14) indicate that the southern Caribbean plate (Site 999) was directly over or near the equator at ~75–80 Ma. Assuming the Galapagos hot spot has maintained its position at ~0.3°S, then the paleolatitude data are consistent with the Caribbean plate passing over the Galapagos hot spot in the Late Cretaceous.

The paleolongitudes, however, indicate that it is unlikely that the Caribbean plate could have been as far west as the Galapagos hot spot (Meschede, 1998; Meschede and Frisch, 1998). For Site 999 to have been at the longitude of Galapagos at 100 Ma and then to move to that position at 80 Ma shown in Figure 16, would require that the Farallon plate move eastward relative to the hot spots at ~130 km/m.y. This rate of eastward motion is roughly two to three times faster than what has been estimated for the motion of the Farallon plate relative to the hot spots during Late Cretaceous time. For example, the average rate of eastward motion of the Farallon plate relative to the hot spots is 64 km/m.y. based on the 74–100 Ma stage pole from Duncan and Hargraves (1984) and is 41 km/m.y. based on the 85- to 100-Ma stage pole from Engebretson et al. (1985).

CONCLUSIONS

Our study provides 18 new paleolatitude estimates from the Caribbean region that span the interval from 81 Ma to the present. These are based on the analysis of over 430 discrete paleomagnetic samples from sedimentary units and 230 measurements made along split-core sections of basalt. Our paleolatitude estimates include corrections that account for a polarity ambiguity bias that occurs when dealing with azimuthally unoriented drill cores that have shallow paleomagnetic inclinations.

Fifteen of the paleolatitude estimates are from Sites 999 and 1001, which lie in the interior of the Caribbean plate. These data provide evidence for the Caribbean plate being positioned near the equator during the Late Cretaceous and then migrating northward to its current position at an average rate of 18 km/m.y. The paleolatitudes estimated in this study are consistent with models that have the Caribbean plate originating either in the Pacific Ocean or in an intra-American position during the Late Cretaceous. In both models, the southern portion of the Caribbean plate (particularly Site 999) would have been within 5° of the equator at ~80 Ma, at ~7.5°N–9°N from 45 to 25 Ma, and would have subsequently moved more rapidly north to the current Site 999 latitude of 12.7°N.

ACKNOWLEDGMENTS

This project was funded by the United States Science Support Program of the Joint Oceanographic Institutions. The manuscript benefitted from the many useful suggestions that were provided by Gren Draper, Katerina Petronotis, and two anonymous reviewers, as well as from the effort of the entire Shipboard Scientific Party during Leg 165. We also thank John Geissman for use of the paleomagnetism laboratory at the University of New Mexico.

REFERENCES

Acton, G., and Gordon, R.G., 1990. A Late Cretaceous paleomagnetic pole for North America from the Fort Hays Limestone. *Eos,* 71:1291.

Arason, P., and Levi, S., 1990a. Compaction and inclination shallowing in deep-sea sediments from the Pacific Ocean. *J. Geophys. Res.,* 95:4501–4510.

————, 1990b. Models of inclination shallowing during sediment compaction. *J. Geophys. Res.,* 95:4481–4500.

Argus, D.F., and Gordon, R.G., 1991. No-net-rotation model of current plate velocities incorporating plate motion model NUVEL-1. *Geophys. Res. Lett.,* 18:2039–2042.

Beck, M.E., 1988. Analysis of Late Jurassic-Recent paleomagnetic data from active plate margins of South America. *J. South Am. Earth Sci.,* 1:39–52.

Boucher, C., Altamimi, Z., Feissel, M., and Sillard, P., 1996. Results and analysis of the ITRF 94. *IERS Tech. Note,* 20. Int. Earth Rotation Serv., Obs. de Paris.

Burke, K., 1988. Tectonic evolution of the Caribbean. *Annu. Rev. Earth Planet. Sci.,* 16:201–230.

Briden, J.C., and Ward, M.A., 1966. Analysis of magnetic inclination in borecores. *Pure Appl. Geophys.,* 57:47–52.

Burmester, R.F., Beck, M.E., Jr., Speed, R.C., and Snoke, A.W., 1996. A preliminary paleomagnetic pole for mid-Cretaceous rocks from Tobago: further evidence for large clockwise rotations in the Caribbean-South American plate boundary zone. *Earth Planet. Sci. Lett.,* 139:79–90.

Celaya, M.A., and Clement, B.M., 1988. Inclination shallowing in deep sea sediments from the North Atlantic. *Geophys. Res. Lett.,* 15:52–55.

Cox, A., and Gordon, R.G., 1984. Paleolatitudes determined from paleomagnetic data from vertical cores. *Rev. Geophys. Space Phys.,* 22:47–72.

DeMets, C., Gordon, R.G., Argus, D.F., and Stein, S., 1994. Effect of recent revisions to the geomagnetic time scale on estimates of current plate motion. *Geophys. Res. Lett.,* 21:2191–2194.

Deng, J., and Sykes, L.R., 1995. Determination of Euler pole for contemporary relative motion of Caribbean and North American plates using slip vectors of interplate earthquakes. *Tectonics,* 14:39–53.

Diehl, J.F., Beck, M.E., Jr., Beske-Diehl, S., Jacobson, D., and Hearn, B.C., Jr., 1983. Paleomagnetism of the Late-Cretaceous-early Tertiary north-central Montana alkalic province. *J. Geophys. Res*., 88:10593–10609.

Diehl, J.F., McClannahan, K.M., and Bornhorst, T.J., 1988. Paleomagnetic results from the Mogollon-Datil volcanic field, southwestern New Mexico, and a refined Mid-Tertiary reference pole for North America. *J. Geophys. Res.,* 93:4869–4879.

Dixon, T.H., Farina, F., DeMets, C., Jansma, P., Mann, P., and Calais, E., 1998. Relative motion between the Caribbean and North American plates and related boundary zone deformation from a decade of GPS observations. *J. Geophys. Res.,* 103:15157–15182.

Draper, G., Jackson, T.A., and Donovan, S.K., 1994. Geologic provinces of the Caribbean region. *In* Donovan, S.K., and Jackson, T.A. (Eds.), *Caribbean Geology: An Introduction: Jamaica*. Univ. West Indies Publ. Assoc., 3–12.

Duncan, R.A., and Hargraves, R.B., 1984. Plate tectonic evolution of the Caribbean region in the mantle reference frame. *In* Bonini, W.E., Hargraves, R.B., and Shagam, R. (Eds.), *The Caribbean-South American Plate Boundary and Regional Tectonics.* Mem.—Geol. Soc. Am., 162:81–94.

Engebretson, D.C., Cox, A., and Gordon, R.G., 1985. *Relative Motions Between Oceanic and Continental Plates in the Pacific Basin.* Spec. Pap.—Geol. Soc. Am., 206.

Frisch, W., Meschede, M., and Sick, M., 1992. Origin of the Central American ophiolites: evidence from paleomagnetic results. *Geol. Soc. Am. Bull.,* 104:1301–1314.

Gordon, R., 1990. Test for bias in paleomagnetically determined paleolatitudes from Pacific Plate Deep Sea Drilling Project sediments. *J. Geophys. Res.,* 95:8397–8404.

Gordon, R.G., 1984. A Paleocene North American paleomagnetic pole incorporating declination-only data. *Geophys. Res. Lett.,* 11:477–480.

————, 1990. Test for bias in paleomagnetically determined paleolatitudes from Pacific plate Deep Sea Drilling Project sediments. *J. Geophys. Res.,* 95:8397–8404.

Gose, W.A., 1983. Late Cretaceous-Early Tertiary tectonic history of southern Central America. *J. Geophys. Res.,* 88:10585–10592.

————, 1985. Caribbean tectonics from a paleomagnetic perspective. *In* Stehli, F.G., and Webb, S.D. (Eds.), *The Great American Biotic Interchange:* New York (Plenum), 285–301.

Gripp, A.E., and Gordon, R.G., 1990. Current plate velocities relative to the hotspots incorporating the NUVEL-1 global plate motion model. *Geophys. Res. Lett.,* 17:1109–1112.

Harrison, C.G.A., 1966. Paleomagnetism of deep sea sediments. *J. Geophys. Res.,* 71:3035–3043.

————, 1980. Secular variation and excursions of the Earth's magnetic field. *J. Geophys. Res.,* 85:3511–3522.

Kent, D.V., 1973. Post-depositional remanent magnetization in deep-sea sediment. *Nature,* 246:32–34.

Kent, D.V., and Spariosu, D.J., 1982. Magnetostratigraphy of Caribbean site 502 hydraulic piston cores. *In* Prell, W.L., Gardner, J.V., et al., *Init. Repts. DSDP,* 68: Washington (U.S. Govt. Printing Office), 419–433.

Kirschvink, J.L., 1980. The least-squares line and plane and the analysis of palaeomagnetic data. *Geophys. J. R. Astron. Soc.,* 62:699–718.

Klitgord, K.D., and Schouten, H., 1986. Plate kinematics of the central Atlantic. *In* Vogt, P.R., and Tucholke, B.E. (Eds.), *The Geology of North America* (Vol. M): *The Western North Atlantic Region.* Geol. Soc. Am., 351–378.

Kono, M., 1980. Statistics of paleomagnetic inclination data. *J. Geophys. Res.,* 85:3878–3882.

Lowrie, W., and Opdyke, N.D., 1973. Paleomagnetism of igneous and sedimentary samples. *In* Edgar, N.T., Saunders, J.B., et al., *Init. Repts. DSDP,* 15: Washington (U.S. Govt. Printing Office), 1017–1022.

MacDonald, W.D., 1990. Survey of Caribbean paleomagnetism. *In* Dengo, G., and Case, J.E. (Eds.), *The Caribbean Region.* Geol. Soc. Am., Geol. of North Am. Ser., H:405–432.

Malfait, B.T., and Dinkelman, M.G., 1972. Circum-Caribbean tectonic and igneous activity and the evolution of the Caribbean plate. *Geol. Soc. Am. Bull.,* 83:251–272.

McFadden, P.L., and Reid, A.B., 1982. Analysis of paleomagnetic inclination data. *Geophys. J. R. Astron. Soc.,* 69:307–319.

Meschede, M., 1998. The impossible Galapagos connection: geometric constraints for a near-American origin of the Caribbean plate. *Geol. Rundsch.,* 87:200–205.

Meschede, M., and Frisch, W., 1998. A plate-tectonic model for the Mesozoic and Early Cenozoic history of the Caribbean plate. *Tectonophysics,* 296:269–291.

Montgomery, H., Pessagno, E.A., Jr., and Pindell, J.L., 1994. A 195 Ma terrane in a 165 Ma sea: Pacific origin of the Caribbean plate. *GSA Today,* 4:1–6.

Morris, A.E.L., Taner, I., Meyerhoff, H.A., and Meyerhoff, A.A., 1990. Tectonic evolution of the Caribbean region: alternative hypothesis. *In* Dengo, G., and Case, J.E. (Eds.), *The Caribbean Region.* Geol. Soc. Am., Geol. of North Am. Ser., H:433–457.

Müller, R.D., Royer, J.Y., and Lawver, L.A., 1993. Revised plate motions relative to the hotspots from combined Atlantic and Indian-Ocean hotspot tracks. *Geology,* 21:275–278.

Opdyke, N.D., 1972. Paleomagnetism of deep-sea cores. *Rev. Geophys. Space Phys.,* 10:213–249.

Opdyke, N.D., and Henry, K.W., 1969. A test of the dipole hypothesis. *Earth Planet. Sci. Lett.,* 6:138–151.

Pindall, J.L., 1994. Evolution of the Gulf of Mexico and the Caribbean, *In* Donovan, S.K., and Jackson, T.A. (Eds.), *Caribbean Geology: An Introduction.* Jamaica (Univ. West Indies Publishers' Assoc.), 13–39.

Pindell, J., Cande, S., Pitman, W., Rowley, D., Dewey, J., Labrecque, J., and Haxby, W., 1988. A plate-kinematic framework for models of Caribbean evolution. *Tectonophysics,* 155:21–138.

Pindall, J.L., and Barrett, S.F., 1990. Geological evolution of the Caribbean region: A plate-tectonic perspective. *In* Dengo, G., and Case, J.E. (Eds.), *The Caribbean Region.* Geol. Soc. Am., Geol. North Am. Ser., H:405–432.

Pindell, J., and Dewey, J., 1982. Permo-Triassic reconstruction of western Pangea and the evolution of the Gulf of Mexico/Caribbean region. *Tectonics,* 1:179–211.

Raff, A., 1973. Site 145. *In* Edgar, N.T., Saunders, J.B., et al., *Init. Repts. DSDP,* 15: Washington (U.S. Govt. Printing Office), 1063–1066.

Sigurdsson, H., Leckie, R.M., Acton, G.D., et al., 1997. *Proc. ODP, Init. Repts.,* 165: College Station, TX (Ocean Drilling Program).

Sykes, L.R., McCann, W.R., and Kafka, A.L., 1982. Motion of Caribbean plate during last 7 million years and implications for earlier Cenozoic movements. *J. Geophys. Res.,* 87:10656–10676.

Tan, X., and Kodama, K.P., 1998. Compaction-corrected inclinations from southern California Cretaceous marine sedimentary rocks indicate no paleolatitudinal offset for the Peninsular Ranges terrane. *J. Geophys. Res.,* 103:27169–27192.

Tarduno, J.A., 1990. Absolute inclination values from deep sea sediments: a reexamination of the Cretaceous Pacific record. *Geophys. Res. Lett.,* 17:101–104.

Date of initial receipt: 29 June 1998
Date of acceptance: 20 April 1999
Ms 165SR-001

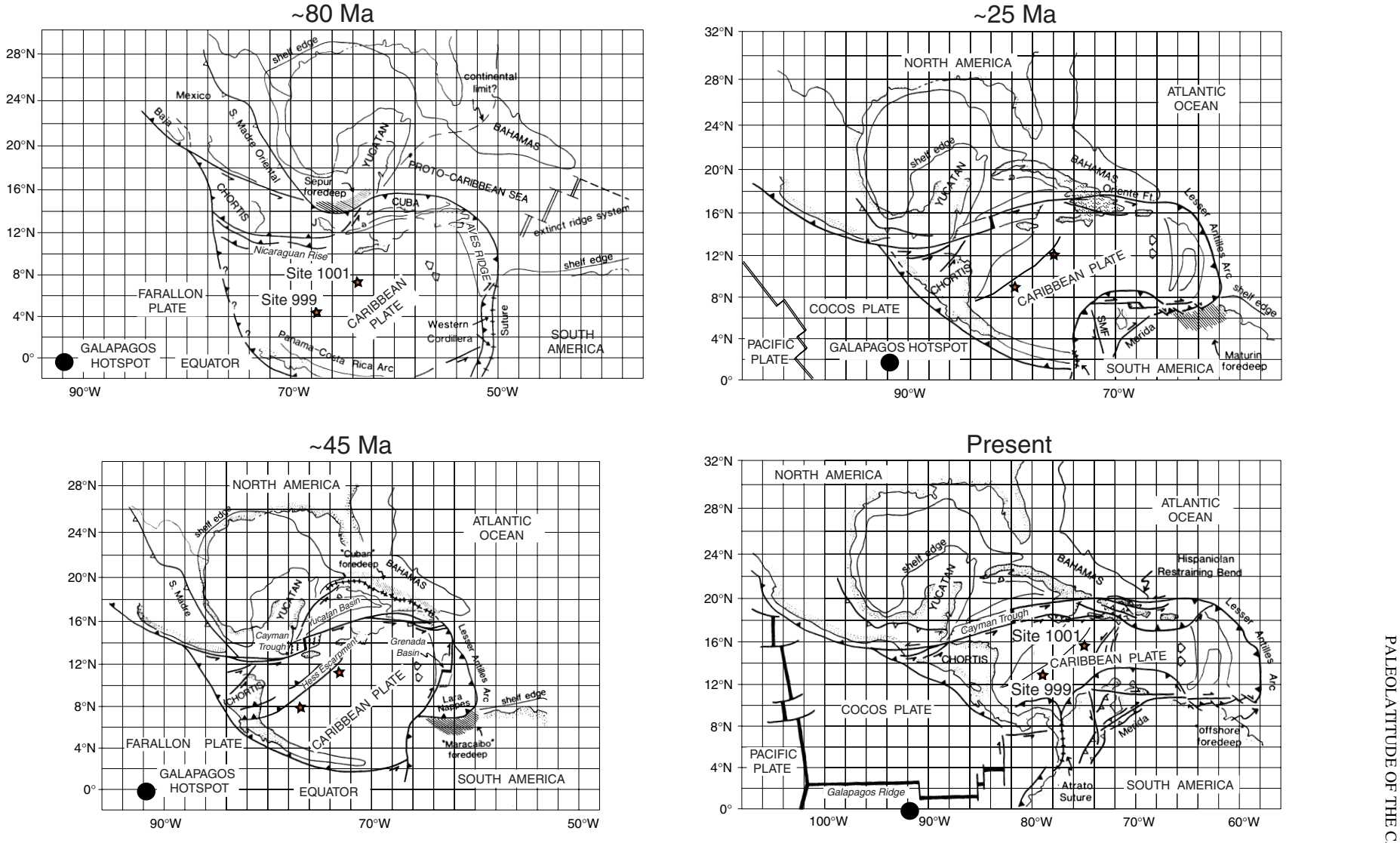

Figure 16. Paleogeographic reconstruction of Pindell et al. (1988) with Leg 165 sites (stars) over a paleogeographic grid. The longitudes of the grid are based on the relative position of North America in the hot-spot reference frame using the reconstruction parameters of Müller et al. (1993). Latitudes of the grid are selected to be consistent with the Caribbean paleomagnetic data, North American paleomagnetic data, and the hot-spot reconstructions.